ADP-23-12/T1221
DESY-23-059
Liverpool LTH 1340
May 9, 2023

Feynman–Hellmann approach to transition matrix elements and quasi-degenerate energy states

M. Batelaan[a], K. U. Can[a], R. Horsley[b], Y. Nakamura[c], P. E. L. Rakow[d], G. Schierholz[e], H. Stüben[f], R. D. Young[a] and J. M. Zanotti[a]

– QCDSF-UKQCD-CSSM Collaboration –

[a] CSSM, Department of Physics, University of Adelaide, Adelaide SA 5005, Australia

[b] School of Physics and Astronomy, University of Edinburgh, Edinburgh EH9 3FD, UK

[c] RIKEN Center for Computational Science, Kobe, Hyogo 650-0047, Japan

[d] Theoretical Physics Division, Department of Mathematical Sciences, University of Liverpool, Liverpool L69 3BX, UK

[e] Deutsches Elektronen-Synchrotron DESY, Notkestr. 85, 22607 Hamburg, Germany

[f] Universität Hamburg, Regionales Rechenzentrum, 20146 Hamburg, Germany

Abstract

The Feynman–Hellmann approach to computing matrix elements in lattice QCD by first adding a perturbing operator to the action is described using the transition matrix and the Dyson expansion formalism. This perturbs the energies in the two-point baryon correlation function, from which the matrix element can be obtained. In particular at leading order in the perturbation we need to diagonalise a matrix of near-degenerate energies. While the method is general for all hadrons, we apply it here to a study of a Sigma to Nucleon baryon transition vector matrix element.

1 Introduction

Quantum Chromodynamics (QCD) – the theory of quarks and gluons has been spectacularly successful in describing inelastic scattering of particles at very high energies, as witnessed in particle accelerators. In this region the coupling constant decreases and allows the application of perturbation theory for quarks and gluons. However at lower energies these bind into hadrons. This is a non-perturbative effect and presently the most successful method to try to describe this is via numerical Monte Carlo simulations of a discretised version of QCD – lattice QCD. While this approach has been pursued from the early days of QCD, it is only recently that computer speeds have improved to such an extent that reasonably accurate numerical results are possible. The general situation of the field is given in [1]. While many early computations were for the mass spectrum, more recently the focus is now on matrix elements, particularly for the nucleon or more generally for the baryon octet[1].

Most of these baryon matrix elements are needed at non-zero momentum transfer. Typical examples are those relevant to lepton–hadron scattering processes leading to form factors, e.g. see [2, 3, 4] for recent reviews, or to inelastic processes such as DIS (deep inelastic scattering) with the associated parton distribution functions, PDFs, e.g. [5, 6] or alternatively via the related hadron tensor or Compton amplitude to give the structure function [7, 8, 9]. (Often the Operator Product Expansion, OPE, is used as it is simpler to determine moments of structure functions, which are also related to matrix elements.) Alternatively matrix elements at low energies for baryon (or meson) semi-leptonic decays are of interest. Indeed these matrix elements are becoming increasingly important, as they provide crucial input into the precision determination of elements of the Cabibbo-Kobayashi-Maskawa (CKM) [10, 11], nuclear physics [12] and the search for beyond-the-standard-model-effects in neutron β-decay, [13, 14, 15, 16], and as such are to be regarded as complementary to searches at the Large Hadron Collider, LHC.

Traditionally matrix elements have been computed from three-point correlation functions. On the lattice these require a (baryon) source and sink together with an operator between them. To avoid excited state contamination and to achieve ground state dominance the distances between the source, operator and sink must be large enough for this to be numerically achieved. However given the lattice sizes at present available and coupled with the fact that higher-point correlation functions are numerically noisier, this can be difficult to achieve. More recently an alternative approach based on the Feynman–Hellmann theorem has emerged [17, 18, 19, 20]. This perturbs the QCD action with a given operator leading to the required matrix element residing in the resulting energy shift. This

[1]While we shall concentrate on the baryon octet in this article, the results presented here are more general and applicable to all hadrons.

can be determined from a two-point correlation function with just a source and sink, rather than a three-point correlation function.

While this approach has been successfully applied to elastic form factors [21], as described in more detail later this needed an application of (degenerate) perturbation theory for matrix elements with baryons having the same energy. While possible, in practice this restricts the approach. In this article we shall generalise previous results from needing degenerate energies to 'near-degenerate' or 'quasi-degenerate' energies. As discussed here this then allows us to consider processes such as the decays of baryons, where it is otherwise difficult to achieve degeneracy of their respective energies.

Derivations of the the Feynman–Hellmann approach can be given based on the 2-point Green's function defined from the partition function, or from the transfer matrix viewpoint. In this article we shall adopt the latter approach. In principle this can allow for a better discussion of the source and sink wavefunctions to be used. In section 2 we briefly describe the transfer matrix technique, mainly to introduce our notation and modification of the QCD Hamiltonian to include a perturbing operator. We shall take the spectrum of the QCD Hamiltonian to have a set of isolated quasi-degenerate energy states. In section 3 we shall consider a two-point baryon correlation function which upon using the Dyson expansion for the transfer matrix leads, for large source–sink separation times t, to the result given in eq. (28), namely a sum of exponential decays in t with coefficients given by various perturbed energies. The energies are related to eigenvalues from the diagonalisation of a matrix in the space of quasi-degenerate states and leads to the phenomenon of 'avoided' energy levels.The simplest case is of two quasi-degenerate states, leading to the solution of a quadratic equation for the eigenvalues. To resolve these energy states we regard the associated 2-point correlation function matrix as a Generalised Eigen-Value Problem, GEVP (equivalent to a variational approach) [22, 23, 24]. (This is further discussed in section 5 when we consider the numerical implementation.) Furthermore, incorporating the spin index, as also discussed in this section, leads to a doubling of the eigenvalue matrix. However, due to the spin structure of the baryon matrix elements under consideration this does not complicate the determination of the eigenvalues significantly.

The results are rather general, and in this article in section 4 and the Appendices we consider several examples. They are all variations where the kinematic geometry is chosen so that initial baryon, B, moves with 3-momentum $\vec{p}$ and the final baryon, B' with momentum $\vec{p}\,' = \vec{p} + \vec{q}$ (or alternatively $\vec{p} - \vec{q}$) where $\vec{q}$ is the momentum transfer chosen such that $E_B(\vec{p}) \approx E_{B'}(\vec{p}\,')$. Taking $B' = B$ for flavour diagonal baryons describes the lepton scattering case, while $B' \neq B$ gives the flavour changing decay case appropriate to investigating weak decays. In section 5 we discuss specific lattice arrangements. We first discuss our proposal for including the (quark) operator in the action and the subsequent matrix inversion. This effectively inserts the operator in quark lines between the source and sink

baryons and so we consider here valence insertions only. (To include sea quarks for flavour diagonal matrix elements would require special purpose generation of configurations or re-weighting with trace estimates.) The explicit example of the vector current decay $\Sigma \to N$, [25, 26, 27, 28], is then considered, whose transition matrix elements are flavour off-diagonal. Some numerical results follow, which we also compare with the conventional 3-point correlation function determination of the matrix element. Section 7 gives our conclusions.

The Appendices give some further details of the methods employed in this article. Appendix A briefly discusses the Euclideanised matrix elements, for completeness, of all local bilinear currents. To evaluate these we need in turn the spinor bilinear terms, which are given in Appendix B. In Appendix C we give an alternative derivation of the energy results including spin for the examples considered here. In Appendix D we describe all the correlation functions needed for this article, while the last appendix (E) gives some more details of the fermion matrix inversion employed here. Preliminary results have appeared in [29].

2 The transfer matrix

2.1 Background

In this article we shall consider the Euclidean 2-point correlation function with a Hamiltonian which includes a perturbing operator with a possible 3-momentum transfer $\vec{q}$

$$\begin{aligned} C_{\lambda B' B}(t) &= \langle \hat{\bar{B}}'(t;\vec{p}\,')\hat{\bar{B}}(0,\vec{0})\rangle_\lambda \\ &\equiv \mathrm{tr}\,[\hat{\bar{B}}'(t;\vec{p}\,')\hat{\bar{B}}(0,\vec{0})\hat{S}_\lambda(\vec{q})^T]\,/\,\mathrm{tr}\,\hat{S}_\lambda(\vec{q})^T\,, \end{aligned} \tag{1}$$

where T is the temporal box size and with $\hat{\bar{B}}(0,\vec{0})$ the initial baryon state at time 0 and spatial origin $\vec{x}_0 = \vec{0}$ together with $\hat{\bar{B}}'(t;\vec{p}\,')$ the final baryon state at time t and momentum $\vec{p}\,'$. Presently we shall ignore any complications arising from the baryon spin structure, and include this later by generalising appropriately the formulae obtained. (Other hadrons, for example mesons, could thus be considered.) The final baryon state[2]

$$\hat{\bar{B}}'(t;\vec{p}\,') = \int_{\vec{x}} e^{-i\vec{p}\,'\cdot\vec{x}}\hat{B}'(t,\vec{x})\,, \tag{2}$$

[2]For simplicity we use a mixture of continuum notation and discrete notation. We shall not consider any possible lattice artifacts effects here. So for example we shall use

$$\frac{(2\pi)^3}{V}\delta^3(\vec{p}-\vec{q}) \equiv \delta_{\vec{p},\vec{q}} = \begin{cases} 1 & \vec{p}=\vec{q} \\ 0 & \vec{p}\neq\vec{q} \end{cases}\,.$$

is a function of momentum $\vec{p}\,'$. We shall not consider any possible lattice discretisation effects in this article, so we shall use a continuum notation in all dimensions. As the initial baryon state is taken at the source position $\vec{x}_0 = \vec{0}$ it contains all momenta and thus

$$\hat{\bar{B}}(0,\vec{0}) = \int_{\vec{p}} \hat{\bar{B}}(0;\vec{p})\,. \tag{3}$$

This arrangement is adopted because when numerically finding the correlation function we invert the Dirac operator for the Green's function on a spatial source point.

The transfer matrix $\hat{S}_\lambda$ is defined by

$$\hat{S}_\lambda(\vec{q}) = e^{-\hat{H}_\lambda(\vec{q})}\,, \tag{4}$$

where we assume the Hamiltonian, $\hat{H}_\lambda$, exists together with the associated complete set of energy eigenstates[3], in particular a unique vacuum state.

We shall consider a perturbed Hamiltonian, here given by

$$\hat{H}_\lambda(\vec{q}) = \hat{H}_0 + \sum_\alpha \lambda_\alpha \hat{\bar{\mathcal{O}}}_\alpha(\vec{q})\,, \tag{5}$$

with momentum $\vec{q}$, as an expansion in λ_α where α is to be regarded as just a label (so for example can be a single Lorentz index or a collection of indices). The perturbing operator $\hat{\bar{\mathcal{O}}}_\alpha(\vec{q})$ is defined by

$$\hat{\bar{\mathcal{O}}}_\alpha(\vec{q}) = \int_{\vec{x}} \left(\hat{O}_\alpha(\vec{x}) e^{i\vec{q}\cdot\vec{x}} + \hat{O}^\dagger_\alpha(\vec{x}) e^{-i\vec{q}\cdot\vec{x}}\right)\,, \tag{6}$$

where $\hat{O}_\alpha(\vec{x})$ may be taken to be a bilinear in the quark fields, i.e. a generalised current, see Appendix A for some more details. $\hat{H}_0$ conserves momentum, but $\hat{H}_\lambda$ only conserves momentum modulo $\vec{q}$. In this form $\hat{\bar{\mathcal{O}}}_\alpha(\vec{q})$ may be taken as Hermitian. Note that in [31] we considered just the case where $\hat{O}_\alpha(\vec{x})$ is also Hermitian. (It is possible to generalise to non-Hermitian operators, see [19], however we shall not consider this further here.) As the previous equations indicate, we are considering operators defined in Euclidean space. The Hermiticity relation for bilinear operators between the Euclidean and Minkowski spaces is also briefly discussed in Appendix A. It is also easy to include covariant derivatives, for example in [32] eq. (23) where the general relation between the Minkowski and Euclidean operators for the vector and axial currents was given. We do not discuss this case further here.

[3]Strictly speaking, even for the unperturbed action considered later here, see section 5.2.3, positivity is lost, but a transfer matrix can still be defined, [30]. Practically this is not a problem and we ignore this point here.

We can also incorporate the generalisation to complex λ by writing λ in polar form, $\lambda_\alpha = |\lambda_\alpha| e^{i\phi_\alpha}$ and absorb the phase into the definition of the operator. Thus we have

$$\begin{aligned} \lambda_\alpha \hat{\tilde{O}}_\alpha(\vec{q}) &\rightarrow \lambda_\alpha \int_{\vec{x}} \hat{O}_\alpha(\vec{x}) e^{i\vec{q}\cdot\vec{x}} + \lambda_\alpha^* \int_{\vec{x}} \hat{O}_\alpha^\dagger(\vec{x}) e^{-i\vec{q}\cdot\vec{x}} \\ &= |\lambda_\alpha| \int_{\vec{x}} (e^{i\phi_\alpha} \hat{O}_\alpha(\vec{x})) e^{i\vec{q}\cdot\vec{x}} + |\lambda_\alpha| \int_{\vec{x}} (e^{i\phi_\alpha} \hat{O}_\alpha(\vec{x}))^\dagger e^{-i\vec{q}\cdot\vec{x}} \,. \end{aligned} \tag{7}$$

This can be useful if we are considering the $O(\lambda^2)$ terms which gives the Compton Amplitude [8, 31, 34], as indicated here in section 3.1 (real λ gives the symmetric part of the amplitude while complex λ enables the antisymmetric part of the Compton Amplitude to be determined). However as we are only interested in the $O(\lambda)$ result here, for simplicity of notation in future we just take λ_α as real. In addition for this case then the index α is redundant, as we are practically just considering one operator. So we shall usually suppress it, but it can easily be reinstated if necessary. (Again, if we are interested in the $O(\lambda^2)$ or higher order terms then the index is relevant, as cross terms of operators appear.)

First using $\hat{\tilde{B}}'(t;\vec{p}) = \hat{S}_\lambda^\dagger(\vec{q})^t \hat{\tilde{B}}'(0;\vec{p}) \hat{S}_\lambda(\vec{q})^t$ and then inserting a complete set of states (in the presence of the perturbation) and taking the temporal box size large picks out the vacuum state and gives the usual result

$$C_{\lambda B'B}(t) = {}_\lambda\langle 0|\hat{\tilde{B}}'(0;\vec{p}')\hat{S}_\lambda(\vec{q})^t \hat{\tilde{B}}(0,\vec{0})|0\rangle_\lambda \,, \tag{8}$$

where $|0\rangle_\lambda$ is the vacuum in the presence of the perturbation and the spectrum of $\hat{H}$ is now normalised with respect to this vacuum. As all the operators are at time $t = 0$, in future we drop this argument. Eq. (8) is the basic equation we shall consider in this article.

2.2 Quasi-degenerate energy states

We shall first derive a general expression, and then consider particular cases. In particular we shall consider discrete degenerate energy states, i.e. $E_{B_r}(\vec{p}_r) = E_{B_s}(\vec{p}_s)$ or near-degenerate energy states $E_{B_r}(\vec{p}_r) \approx E_{B_s}(\vec{p}_s)$, both possibilities labelled by $r = 1, 2, \ldots$ (similarly for s) each with a given fixed momentum. Collectively we call this set S of 'quasi-degenerate energy' states, the total number being d_S.

In this scenario, as we shall see, simple perturbation theory as it stands breaks down and we have to consider degenerate perturbation theory. This also ensures smooth behaviour in λ. In the following we shall assume that these energy states are the only possible quasi-degenerate states and well separated from other states, as sketched in Fig. 1. We shall later argue that other states are either more damped (those with higher energies in the figure), or for any lower state(s) a GEVP must be applied. However in this article we will only consider the quasi-degenerate energy states as the ground states.

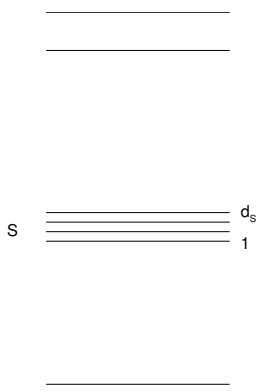

Figure 1: A sketch of the energy levels. The set of quasi-degenerate energy states are denoted by S, labelled from 1 to d_S. These states are well separated from other states.

The spectrum of the unperturbed Hamiltonian, $\hat{H}_0$, is given by

$$\hat{H}_0|X(\vec{p}_X)\rangle = E_X(\vec{p}_X)|X(\vec{p}_X)\rangle\,. \tag{9}$$

Let S be the discrete set of quasi-degenerate energy states and have d_S elements labelled by r. More concretely we write for these states

$$E_{B_r}(\vec{p}_r) = \bar{E} + \epsilon_r\,, \qquad r = 1\,,\ldots\,,d_S\,, \tag{10}$$

where $\bar{E}$ is some suitable energy close to all the quasi-degenerate energies. It could be taken as the average over the quasi-degenerate energy states $\bar{E} = (E_{B_1} + \ldots + E_{B_{d_S}})/d_S$ where we would have $\epsilon_1 + \ldots + \epsilon_{d_S} = 0$ but this is not necessary in the following. (Alternatively we could choose one of the quasi-degenerate energy states, such as the one with lowest energy.) Writing $\epsilon_r = \epsilon c_r$ where $c_r \sim O(1)$ then $\epsilon \sim |E_{B_r}(\vec{p}_r) - E_{B_s}(\vec{p}_s)|$ effectively represents the difference in energies between the quasi-degenerate states where ϵ is small and is taken in the following to be another expansion parameter in addition to λ. The corresponding states are denoted by $|B_r(\vec{p}_r)\rangle$. For these quasi-degenerate states we have the energies $E_{B_r}(\vec{p}_r)$ defined by

$$\hat{H}_0|B_r(\vec{p}_r)\rangle = E_{B_r}(\vec{p}_r)|B_r(\vec{p}_r)\rangle\,. \tag{11}$$

The set of unperturbed states obeys the completeness condition where we sum over all states and momenta. We often explicitly isolate the quasi-degenerate states so

$$\not{\sum\!\!\!\!\!\!\int}_{X(\vec{p}_X)} |X(\vec{p}_X)\rangle\langle X(\vec{p}_X)| \equiv \sum_r |B_r(\vec{p}_r)\rangle\langle B_r(\vec{p}_r)| + \not{\sum\!\!\!\!\!\!\int}_{X(\vec{p}_X)\notin S} |X(\vec{p}_X)\rangle\langle X(\vec{p}_X)| = \hat{1}\,. \tag{12}$$

We use the lattice normalisation, namely

$$\langle X(\vec{p}_X)|Y(\vec{p}_Y)\rangle = \delta_{X,Y}\,\delta_{\vec{p}_X,\vec{p}_Y}\,. \tag{13}$$

However all the formulae and results are such that they can be easily converted to another normalisation by the substitution for all states

$$|X(\vec{p}_X)\rangle \to \frac{|X(\vec{p}_X)\rangle}{\sqrt{\langle X(\vec{p}_X)|X(\vec{p}_X)\rangle}}\,, \qquad |0\rangle \to |0\rangle\,. \tag{14}$$

The usual case, of course, is the relativistic normalisation

$$\langle X(\vec{p}_X)|Y(\vec{p}_Y)\rangle_{\rm rel} = 2E_X(\vec{p}_X)\delta_{X,Y}\delta_{\vec{p}_X,\vec{p}_Y}\,, \tag{15}$$

which we shall later use when discussing the numerical results.

Now inserting two complete sets of unperturbed states before and after $\hat{S}_\lambda^t$ in eq. (8) gives

$$C_{\lambda\,B'B}(t) = \tag{16}$$
$$\sum\!\!\!\!\!\!\int_{X(\vec{p}_X)} \sum\!\!\!\!\!\!\int_{Y(\vec{p}_Y)} {}_\lambda\langle 0|\hat{\bar{B}}'(\vec{p}')|X(\vec{p}_X)\rangle\,\langle X(\vec{p}_X)|\hat{S}_\lambda(\vec{q})^t|Y(\vec{p}_Y)\rangle\,\langle Y(\vec{p}_Y)|\hat{\bar{B}}(\vec{0})|0\rangle_\lambda\,.$$

From eq. (2), as $\hat{B}'$ has a definite momentum, $\vec{p}'$, we can take the geometry to be such that we have a good overlap with just one of the d_S quasi-degenerate states $|B_r(\vec{p}_r)\rangle$ as depicted in Fig. 1. For $\hat{B}(\vec{0})$ we also choose an operator with a good overlap with one of the quasi-degenerate states noting that it contains all momenta. We shall further discuss this in the next section, but initially we shall keep the operators general.

3 Dyson series and the correlation function

3.1 Perturbed energies

We wish to determine $C_{\lambda\,B'B}(t)$ to $O(\lambda)$. To this end, first for any two operators $\hat{A}$, $\hat{B}$ consider the function defined by $f(t) = e^{-t\hat{A}}e^{t(\hat{A}+\hat{B})}$. By the usual technique of differentiating and then integrating $f(t)$ with respect to t we soon find the operator identity

$$e^{t(\hat{A}+\hat{B})} = e^{t\hat{A}} + \int_0^t dt'\, e^{(t-t')\hat{A}}\hat{B}\,e^{t'(\hat{A}+\hat{B})}\,. \tag{17}$$

Regarding $\hat{B}$ as 'small', this can be iterated. From eq. (5) we thus set $\hat{A} \to -\hat{H}_0$ and $\hat{B} \to -\lambda_\alpha\hat{\bar{\mathcal{O}}}_\alpha$. This gives to $O(\lambda^2)$,

$$\begin{aligned} e^{-(\hat{H}_0-\lambda_\alpha\hat{\bar{\mathcal{O}}}_\alpha)t} \;=\; & e^{-\hat{H}_0t} - \lambda_\alpha\int_0^t dt'\, e^{-\hat{H}_0(t-t')}\,\hat{\bar{\mathcal{O}}}_\alpha\, e^{-\hat{H}_0t'} \\ & + \lambda_\alpha\lambda_\beta\int_0^t dt'\int_0^{t'} dt''\, e^{-\hat{H}_0(t-t')}\,\hat{\bar{\mathcal{O}}}_\alpha\, e^{\hat{H}_0(t'-t'')}\,\hat{\bar{\mathcal{O}}}_\beta e^{-\hat{H}_0t''} \\ & + O(\lambda^3)\,, \end{aligned} \tag{18}$$

which is equivalent to the Dyson expansion. We note that the term quadratic in λ can be manipulated into a form appropriate for the Compton amplitude. An alternative derivation using the path integral is discussed in [8, 31]. A recent review is given in [33]. For the specific approach using the transfer matrix given here see also [34].

To evaluate $C_{\lambda B'B}(t)$ we apply the Dyson expansion of eq. (18) to eq. (16) after splitting the completeness relation as given in eq. (12). As mentioned before we shall consider the case where E_X (and E_Y) are much greater than all the isolated quasi-degenerate states as depicted in Fig. 1, i.e. $E_X, E_Y \gg \bar{E}$ in eq. (12). There are four terms and dropping temporarily the momentum arguments gives

$$\begin{aligned}
\langle B_r|e^{-(\hat{H}_0+\lambda\hat{\tilde{\mathcal{O}}})t}|B_s\rangle &= e^{-\bar{E}t}\left(\delta_{rs} - tD_{rs} + O(2)\right), \\
\langle B_r|e^{-(\hat{H}_0+\lambda\hat{\tilde{\mathcal{O}}})t}|Y\rangle &= -e^{-\bar{E}t}\left(\lambda\frac{\langle B_r|\hat{\tilde{\mathcal{O}}}|Y\rangle}{E_Y - E_{B_r}} + O(2)\right) + \begin{matrix}\text{more}\\ \text{damped}\end{matrix}, \\
\langle X|e^{-(\hat{H}_0+\lambda\hat{\tilde{\mathcal{O}}})t}|B_s\rangle &= -e^{-\bar{E}t}\left(\lambda\frac{\langle X|\hat{\tilde{\mathcal{O}}}|B_s\rangle}{E_X - E_{B_s}} + O(2)\right) + \begin{matrix}\text{more}\\ \text{damped}\end{matrix}, \\
\langle X|e^{-(\hat{H}_0+\lambda\hat{\tilde{\mathcal{O}}})t}|Y\rangle &= \begin{matrix}\text{more}\\ \text{damped}\end{matrix},
\end{aligned} \tag{19}$$

where we have defined the $d_S \times d_S$ matrix[4]

$$D_{rs} = \epsilon_r\delta_{rs} + \lambda a_{rs}, \quad \text{with} \quad a_{rs} = \langle B_r(\vec{p}_r)|\hat{\tilde{\mathcal{O}}}(\vec{q})|B_s(\vec{p}_s)\rangle. \tag{20}$$

Note that from eq. (10) we have $\epsilon_r = E_{B_r} - \bar{E}$. In eq. (19) "more damped" means that these terms drop off as $\propto e^{-E_X t}$, i.e. faster then $e^{-\bar{E}t}$. The kept terms (i.e. D) means terms of the form $O(1)$ or $O(\epsilon t)$, $O(\lambda t)$ while $O(2)$ means terms of the form $O(\epsilon^2t^2)$, $O(\lambda^2t^2)$, $O(\epsilon t\lambda t)$. Thus for this expansion to be valid we need $\lambda t \ll 1$, $|\epsilon_r|t \ll 1$ and $t \gg 0$ (for the damped terms to be negligible) thus

$$0 \ll t \ll \frac{1}{\lambda}, \qquad \text{and} \qquad 0 \ll t \ll \frac{1}{\max|E_{B_r}(\vec{p}_r) - E_{B_s}(\vec{p}_s)|}. \tag{21}$$

Furthermore defining $|B_s(\vec{p}_s)\rangle_\lambda$ as

$$|B_s(\vec{p}_s)\rangle_\lambda = |B_s(\vec{p}_s)\rangle - \lambda \sum\!\!\!\!\!\!\int_{E_Y \gg \bar{E}} |Y(\vec{p}_Y)\rangle \frac{\langle Y(\vec{p}_Y)|\hat{\tilde{\mathcal{O}}}(\vec{q})|B_s(\vec{p}_s)\rangle}{E_Y - E_{B_s}}, \tag{22}$$

then we can re-write eq. (16) as

$$\begin{aligned}
&C_{\lambda B'B}(t) \\
&\quad = \sum_{rs} {}_\lambda\langle 0|\hat{\tilde{B}}'(\vec{p}')|B_r(\vec{p}_r)\rangle_\lambda \, \langle B_r|e^{-(\hat{H}_0+\lambda\hat{\tilde{\mathcal{O}}})t}|B_s\rangle \, {}_\lambda\langle B_s(\vec{p}_s)|\hat{\tilde{B}}(\vec{0})|0\rangle_\lambda,
\end{aligned} \tag{23}$$

[4] D is a function of the momenta, but as with $C_{\lambda B'B}(t)$ we shall suppress this dependence.

where

$$\langle B_r(\vec{p}_r)|e^{-(\hat{H}_0+\lambda\hat{\tilde{\mathcal{O}}})t}|B_s(\vec{p}_s)\rangle = (\delta_{rs} - tD_{rs}) \times e^{-\bar{E}t} \,. \tag{24}$$

Note that we have achieved a factorisation where any unwanted $|Y\rangle$ states, with $E_Y \gg E_{B_s}$, have been absorbed into the time independent renormalisation of the wavefunction and do not need to be further considered.

The matrix D given in eq. (20) can be diagonalised, as it is Hermitian by construction. Let $\mu^{(i)}$ be the real eigenvalues and $e_r^{(i)}$ the associated orthonormal d_S dimensional eigenvectors

$$\sum_{i=1}^{d_S} e_r^{(i)} e_s^{(i)\,*} = \delta_{rs} \,, \qquad \sum_{r=1}^{d_S} e_r^{(i)\,*} e_r^{(j)} = \delta^{ij} \,. \tag{25}$$

Thus we have

$$D_{rs} = \sum_{i=1}^{d_S} \mu^{(i)} e_r^{(i)} e_s^{(i)\,*} \,. \tag{26}$$

(Note that to find the eigenvalues we have to first solve a d_S-dimensional polynomial.) So all together using this in eq. (24) we find the intermediate result

$$\langle B_r|e^{-(\hat{H}_0+\lambda\hat{\tilde{\mathcal{O}}})t}|B_s\rangle = \sum_{i=1}^{d_S} e_r^{(i)} \left[1 - t\mu^{(i)}\right] e_s^{(i)\,*} \times e^{-\bar{E}t} \,, \tag{27}$$

which we now use to find the final form of the correlation function.

3.2 The correlation function

3.2.1 General result

Finally, we re-exponentiate the first term in eq. (27) and then substitute back into eq. (23) to give the leading term at large t of

$$C_{\lambda B' B}(t) = \sum_{i=1}^{d_S} A^{(i)}_{\lambda B' B}\, e^{-E^{(i)}_\lambda t} \,, \tag{28}$$

where the perturbed energies are given by

$$E^{(i)}_\lambda = \bar{E} + \mu^{(i)} \,, \tag{29}$$

and the amplitude

$$A^{(i)}_{\lambda B' B} = w^{(i)}_{B'} \bar{w}^{(i)}_{B} \,, \tag{30}$$

with

$$w^{(i)}_{B'} = \sum_{r=1}^{d_S} Z^{B'}_r e^{(i)}_r \,, \quad \text{and} \quad \bar{w}^{(i)}_{B} = \sum_{s=1}^{d_S} \bar{Z}^{B}_s e^{(i)*}_s \,, \tag{31}$$

where the wavefunctions, or overlaps, are

$$Z_r^{B'} = {}_\lambda\langle 0|\hat{\bar{B}}'(\vec{p}')|B_r(\vec{p}_r)\rangle_\lambda \quad \text{and} \quad \bar{Z}_s^{B} = {}_\lambda\langle B_s(\vec{p}_s)|\hat{\bar{B}}(\vec{0})|0\rangle_\lambda \,. \tag{32}$$

Eqs. (28) – (32) are the results that we shall be using in the following.

In the final/initial baryon space, $\{B', B\}$, the determination of $E_\lambda^{(i)}$, $i = 1, \ldots, d_S$ is now equivalent to a GEVP, where we diagonalise a matrix of correlation functions. To determine all the energies we thus require this to be at least a $d_S \times d_S$ matrix, so both the sets $\{B'\}$ and $\{B\}$ must be at least d_S dimensional.

If there were states $|Z\rangle$ with lower energy than the quasi-degenerate energy states and hence less damped than these states then the $\{B', B\}$ space must be increased and a larger GEVP applied. We do not consider this lower energy case further here, and take the quasi-degenerate energy states to be the lowest states. Additionally, if the higher energy states have not died away sufficiently then a larger $\{B', B\}$ space could also be used.

3.2.2 A simplification

The above result is true for general source and sink operators. If as mentioned before, we set $\hat{B}'$ and $\hat{B}$ 'close' to $\hat{B}_r$ and $\hat{B}_s$ respectively then the above expressions greatly simplify and we expect that eq. (31) reduces to

$$w_r^{(i)} = Z_r^{B_r} e_r^{(i)} \,, \quad \text{and} \quad \bar{w}_s^{(i)} = \bar{Z}_s^{B_s} e_s^{(i)*} \,. \tag{33}$$

In turn this means that the overlaps $Z_r^{B_r}$ and $\bar{Z}_s^{B_s}$ although defined using the perturbed states of eq. (22), the $O(\lambda)$ terms have then little effect. For example for $Z_r^{B_r}$ using eq. (22)[5] to expand ${}_\lambda\langle 0|\hat{\bar{B}}_r(\vec{p}_r)|B_r(\vec{p}_r)\rangle_\lambda$ the $O(\lambda)$ terms which involve overlaps such as $\langle 0|\hat{B}_r|Y\rangle$ or $\langle X|\hat{B}_r|B_r\rangle$ vanish or are small due to the orthogonality of the spectrum, so the effect of the perturbation on the overlaps is higher order in λ. We thus have

$$Z_r^{B_r} = \langle 0|\hat{B}_r(\vec{0})|B_r(\vec{p}_r)\rangle + \ldots \quad \text{and} \quad \bar{Z}_s^{B_s} = \langle B_s(\vec{p}_s)|\hat{\bar{B}}_s(\vec{0})|0\rangle + \ldots \,. \tag{34}$$

where in addition for $Z_r^{B_r}$ we have also used $\hat{B}(\vec{x}) = e^{-i\hat{\vec{p}}\cdot\vec{x}}\, \hat{B}(\vec{0})\, e^{i\hat{\vec{p}}\cdot\vec{x}}$ to re-write it in the above form.

3.3 The relation between the initial and final momenta

While the equations in section 3.2 are the basic results, this discussion is general and can be applied to many quantum systems. We shall now be more specific to the situation here. However before considering some examples we shall first

[5] We shall assume that this also holds for the perturbed vacuum, $|0\rangle_\lambda$.

discuss some properties of the matrix element appearing in eq. (20). Using $\hat{O}(\vec{x}) = e^{-i\hat{\vec{p}}\cdot\vec{x}}\,\hat{O}(\vec{0})\,e^{i\hat{\vec{p}}\cdot\vec{x}}$ we soon find

$$\begin{aligned}&\langle B_r(\vec{p}_r)|\hat{\tilde{\mathcal{O}}}(\vec{q})|B_s(\vec{p}_s)\rangle \\ &\quad = \langle B_r(\vec{p}_r)|\hat{O}(\vec{0})|B_s(\vec{p}_s)\rangle\,\delta_{\vec{p}_r,\vec{p}_s+\vec{q}} + \langle B_r(\vec{p}_r)|\hat{O}^\dagger(\vec{0})|B_s(\vec{p}_s)\rangle\,\delta_{\vec{p}_r,\vec{p}_s-\vec{q}}\,.\end{aligned} \tag{35}$$

Thus the initial momentum, $\vec{p}_s$ either steps up or down by $\vec{q}$, i.e.

$$\vec{p}_r = \vec{p}_s + \vec{q}\,, \quad \text{or} \quad \vec{p}_r = \vec{p}_s - \vec{q}\,, \tag{36}$$

and the quasi-degenerate states, as sketched in Fig. 1, are mixed together.

As a simple example, to be discussed in some detail in section 4, let us take the two dimensional quasi-degenerate state subspace as having momentum $\vec{p}$ and $\vec{p}+\vec{q}$. Thus the final momentum $\vec{p}_r$ can be chosen to be either $\vec{p}_r = \vec{p}+\vec{q}$ with the + sign and $\vec{p}_s = \vec{p}$ (or $\vec{p}_r = \vec{p}-\vec{q}$ with the − sign and $\vec{p}_s = \vec{p}$) to remain within this subspace. We shall use these results frequently in the coming presentation.

A corollary from eq. (35) is that for a non-zero momentum transfer, $\vec{q} \neq 0$, the diagonal matrix elements a_{rr} in eq. (20) are zero, so the $O(\lambda)$ terms vanish and hence D becomes trivial. This was alluded to before: if we are investigating momentum transfer and form factors, then we are forced to consider the degenerate energy case to determine the matrix element [21]. Non-zero off-diagonal matrix elements leads to the phenomenon of avoided energy levels, as discussed later in section 4.

As well as degeneracies between levels differing in momentum by $\pm\vec{q}$ there will also be cases where states differing by $\pm 2\vec{q}$, $\pm 3\vec{q}$ etc. are nearly degenerate. Such degeneracies will be converted into avoided level crossings by the operator acting multiple times. (These are determined by higher orders in λ of the Dyson expansion in eq. (18).) We have not investigated these higher order cases here.

3.4 Incorporating the spin index

We now consider the complications caused by the spinor index and the consequent spin-1/2 carried by the octet baryons. Until now we have postponed this discusion, so strictly the previous results correspond to spinless scalar particles. To incorporate the spin index, σ and the corresponding Dirac index α we shall see that this involves an alternative approach to that usually used when computing 3-point correlation functions. We first generalise eqs. (23) and (24) appropriately and together with $\hat{B}' \sim \hat{B}_r$ and $\hat{B} \sim \hat{B}_s$ this gives

$$\begin{aligned}&C_{\lambda\, B_{r\alpha}\, B_{s\beta}}(t) \\ &\quad = \sum_{\sigma_r\sigma_s} {}_\lambda\langle 0|\hat{\tilde{B}}_{r\alpha}(\vec{p}_r)|B_r(\vec{p}_r,\sigma_r)\rangle_\lambda \times \\ &\qquad\qquad \langle B_r(\vec{p}_r,\sigma_r)|e^{-(\hat{H}_0+\lambda\hat{\tilde{\mathcal{O}}})t}|B_s(\vec{p}_s,\sigma_s)\rangle \times {}_\lambda\langle B_s(\vec{p}_s,\sigma_s)|\hat{\tilde{B}}_{s\beta}(\vec{0})|0\rangle_\lambda\,,\end{aligned} \tag{37}$$

where

$$\langle B_r(\vec{p}_r,\sigma_r)|e^{-(\hat{H}_0+\lambda\hat{\tilde{\mathcal{O}}})t}|B_s(\vec{p}_s,\sigma_s)\rangle \;=\; (\delta_{\sigma_r\sigma_s}\delta_{rs} - tD_{\sigma_r r,\sigma_s s})\times e^{-\bar{E}t}\,, \tag{38}$$

and

$$D_{r\sigma_r,s\sigma_s} = \epsilon_r\delta_{\sigma_r\sigma_s}\delta_{rs} + \lambda a_{\sigma_r r,\sigma_s s}\,, \tag{39}$$

where we have now defined $a_{\sigma_r r,\sigma_s s}$ as the matrix element

$$a_{\sigma_r r,\sigma_s s} = \langle B_r(\vec{p}_r,\sigma_r)|\hat{\tilde{\mathcal{O}}}(\vec{q})|B_s(\vec{p}_s,\sigma_s)\rangle\,. \tag{40}$$

As the spin $\sigma_r = \pm$ the D matrix is doubled in size, now being a $2d_S\times 2d_S$ matrix, i.e. the r index is interlaced in $\pm$ pairs. The matrix element is defined with respect to $\hat{H}_0$ and we expect that the energies corresponding to the spin states $|B(\vec{p},\sigma)\rangle$, with $\sigma = \pm$ are degenerate. (This is a reflection of Kramers degeneracy.)

We could continue as before with this enlarged matrix. However it is simplest to try to keep as close as possible to the previous results. We can achieve this by writing the overlaps as

$$\begin{aligned} {}_\lambda\langle 0|\hat{B}_{r\,\alpha}(\vec{0})|B_r(\vec{p}_r,\sigma_r)\rangle_{\lambda\,\mathrm{rel}} &= Z_r\, u^{(r)}_\alpha(\vec{p}_r,\sigma_r) + \ldots\,, \\ {}_\lambda\langle B_s(\vec{p}_s,\sigma_s)|\hat{\bar{B}}_{s\,\beta}(\vec{0})|0\rangle_{\lambda\,\mathrm{rel}} &= \bar{Z}_s\,\bar{u}^{(s)}_\beta(\vec{p}_s,\sigma_s) + \ldots\,, \end{aligned} \tag{41}$$

where Z_r and $\bar{Z}_s$ are taken as scalars with $\bar{Z} = Z^*$. Although the states here are the perturbed states, rather then the unperturbed states, again we expect the effect of the perturbation to be small, as discussed in section 3.2.2.

Furthermore, although we could consider the Dirac indices as a GEVP it is more convenient to sum over them with some matrix, Γ. In this article we shall primarily consider the unpolarised case with

$$\Gamma^{\mathrm{unpol}} = (1+\gamma_4)/2\,, \tag{42}$$

so

$$C_{\lambda\,rs}(t) = \mathrm{tr}\Gamma^{\mathrm{unpol}}C_{\lambda\,B_rB_s}(t)\,. \tag{43}$$

Using

$$\bar{u}^{(r)}(\vec{p}_r,\sigma_r)\Gamma^{\mathrm{unpol}}u^{(s)}(\vec{p}_s,\sigma_s) = \sqrt{(E_r+M_r)(E_s+M_s)}\,\delta_{\sigma_r\sigma_s}\,, \tag{44}$$

(see Appendix B and eq. (108)) means that due to the $\delta_{\sigma_r\sigma_s}$ term appearing there, the σ_r, σ_s sums in eq. (37) become diagonal, and hence we just sum over them in eqs. (38), (39). This reduces D to the previous $d_S\times d_S$ matrix as in section 3.2, where

$$D_{rs} = \epsilon_r\delta_{rs} + \lambda a_{rs}\,, \quad \text{with} \quad a_{rs} = \frac{1}{2}(a_{+r,+s} + a_{-r,-s})\,. \tag{45}$$

This effectively is the same result as before, but we are now just averaging over the diagonal spin terms. This gives finally

$$C_{\lambda rs}(t) = \sum_{i=1}^{d_S} w_r^{(i)} \bar{w}_s^{(i)} e^{-E_\lambda^{(i)} t} \,, \tag{46}$$

with[6]

$$w_r^{(i)} = Z_r e_r^{(i)} \quad \text{and} \quad \bar{w}_s^{(i)} = \bar{Z}_s e_s^{(i)\,*} \,, \tag{47}$$

where the eigenvectors, $e_r^{(i)}$ are from the D matrix in eq. (45) and the eigenvalues $\mu^{(i)}$ give the energies $E_\lambda^{(i)} = \bar{E} + \mu^{(i)}$ as in eq. (29).

Another possibility is $\Gamma^{\rm pol}_{\pm 3} = (1+\gamma_4)/2 \times (1 \pm i\gamma_5\gamma_3)$ (see Appendix B.2.2 and eq. (109)) which again gives a reduced D_{rs} together with $a_{rs} = a_{\pm r,\pm s}$. (Note that both these Γ-matrix forms are chosen so that the diagonal $\delta_{\sigma_r\sigma_s}\delta_{rs}$ term in eq. (38) remains as δ_{rs}.) The choice of projection matrix, Γ, depends on the symmetry of the operator and picks out the relevant matrix element. So, as discussed here for an unpolarised or spin-non-flip matrix element we would use $\Gamma^{\rm unpol}$ or $\Gamma^{\rm pol}_{\pm 3}$.

In Appendix A (together with Appendix B) we have investigated the phase factor relationship between $a_{-r,-s}$ with $a_{+r,+s}$ (or $a_{-r,+s}$ with $a_{+r,-s}$) for all possible local bilinear currents culminating in eq. (88) and Table 3.

Furthermore in Appendix C, as a check, the general result for the spin-non-flip $d_S = 2$ case considered here is given. Some comments are also made for the spin-flip case using for example $\Gamma^{\rm pol}_{\pm} = (1+\gamma_4)/2 \times i\gamma_5(\gamma_1 \pm i\gamma_2)$ which cannot be put in the form discussed in this section (i.e. as an effective D_{rs}).

4 Quasi-degenerate baryon energy states

4.1 Flavour diagonal matrix elements

The simplest example, as alluded to in section 3.3, is to consider two close energy states for the same baryon but with different momentum. Thus the possible operators in eq. (6) must be flavour diagonal. (We shall consider flavour changing, that is flavour off-diagonal matrix elements in the next section.) To be concrete we shall consider the nucleon, $B = N(uud)$ here, although the results hold for

[6]For notational simplicity we have have absorbed some factors into a redefinition of the overlap definitions

$$\sqrt{\frac{E_r + M_r}{E_r}}\, Z_r \to Z_r \,, \quad \text{and} \quad \sqrt{\frac{E_s + M_s}{E_s}}\, \bar{Z}_s \to \bar{Z}_s \,.$$

This is due to to the relativistic normalisation, eq. (15), used for the results in Appendix B, together with eq. (44) and a factor 2 from the averaging over polarisations.

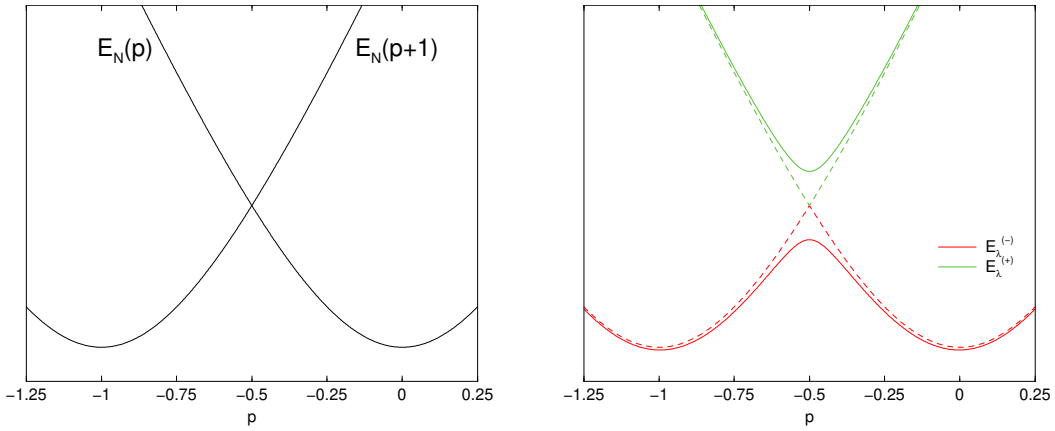

Figure 2: LH panel: A sketch of the (unperturbed) energy states $E_N(p)$, $E_N(p+q)$ versus p in one dimension for fixed q using units where $q = 1$. Using these units there is a degeneracy at $p = -1/2$. RH panel: An equivalent sketch of the perturbed energy states, $E^{(\pm)}$ based on eq. (53). The dashed lines are the free case. The sketch shows the avoided energy levels.

other octet (or decuplet) particles. As an example, we may take the quark content of the operator to be

$$O(\vec{x}) \sim (\bar{u}\gamma u)(\vec{x}) - (\bar{d}\gamma d)(\vec{x})\,, \tag{48}$$

where γ is an arbitrary Dirac gamma matrix. As discussed previously we shall first consider the general structure and then finally incorporate the spin index as in section 3.4.

Clearly we have a degeneracy or near degeneracy when $\vec{q}$ is chosen such that we have the energy states with $E_N(\vec{p}) \approx E_N(\vec{p}+\vec{q})$ (or alternatively $E_N(\vec{p}) \approx E_N(\vec{p}-\vec{q})$). Let us now consider some possible solutions focusing on $E_N(\vec{p}) \approx E_N(\vec{p}+\vec{q})$. For clarity we first describe this for the the non-interacting case, later we generalise to the interacting case, leading to an avoided level crossing.

Let us first consider the simpler 1-dimensional case (for example suppose that $\vec{q}$ is in the z-direction: $\vec{q} = (0,0,q)$ and similarly for $\vec{p}$). There will now be a crossing at $p = -q/2$ where $p^2 = (p+q)^2$ and we would have a near-degenerate state close to these states. These are illustrated in the left hand, LH, panel in Fig. 2 where a sketch of the crossing is shown. This is the region we wish to consider perturbation theory by applying the Feynman–Hellmann theorem – well separated from other potential degeneracies. In 3-dimensions we have the corresponding simple solution $\vec{p} = -\vec{q}/2$. This possibility was considered in [21].

In the following, we derive results close to (or at) the degeneracies. We shall only consider 2-fold degeneracies as this means that $d_S = 2$ and we have a quadratic eigenvalue equation to solve. (The doubling to include the spin index, as previously discussed in section 3.4 is a simple generalisation and will be stated at the end of this section.) While we can solve higher dimensional polynomials, they are likely to be less useful as the result will contain several different

nucleon matrix elements, which are difficult to disentangle. Note that this requirement becomes more difficult to achieve if $\vec{q}$ is too small as the λ range where D in eq. (20) takes the form of a 2×2 matrix might become rather narrow, forcing the use of higher dimensional D matrices.

After this general discussion let us take the two momenta to be $\vec{p}$ and $\vec{p}+\vec{q}$ and we consider the case where the two degenerate states form the subspace where $E_N(\vec{p}+\vec{q}) \approx E_N(\vec{p})$. So we set

$$|B_1(\vec{p}_1)\rangle = |N(\vec{p})\rangle\,, \qquad |B_2(\vec{p}_2)\rangle = |N(\vec{p}+\vec{q})\rangle\,, \tag{49}$$

with $E_{B_1}(\vec{p}_1) \equiv E_N(\vec{p}) = \bar{E} + \epsilon_1$ and $E_{B_2}(\vec{p}_2) \equiv E_N(\vec{p}+\vec{q}) = \bar{E} + \epsilon_2$. The geometry of $\vec{p}$ and $\vec{q}$ is chosen so that $E_N(\vec{p}+\vec{q}) \approx E_N(\vec{p})$ are the lowest energy states in this sector, i.e. there is no state with a lower energy, as indicated in the LH panel of Fig. 2. Momentum conservation, i.e. the step-up or step-down in $\vec{q}$ from eq. (35) gives the matrix of baryon matrix elements as

$$a_{rs} = \langle B_r(\vec{p}_r)|\hat{\bar{O}}(\vec{q})|B_s(\vec{p}_s)\rangle = \begin{pmatrix} 0 & a^* \\ a & 0 \end{pmatrix}_{rs}\,, \tag{50}$$

where

$$a = \langle B_2(\vec{p}_2)|\hat{O}(\vec{0})|B_1(\vec{p}_1)\rangle\,. \tag{51}$$

To first find the eigenvalues of D in eq. (20) we have to solve a quadratic equation. This gives

$$\mu^{(\pm)} = \frac{1}{2}(\epsilon_1+\epsilon_2) \pm \frac{1}{2}\sqrt{(\epsilon_1-\epsilon_2)^2 + 4\lambda^2|a|^2}\,. \tag{52}$$

leading to the energies

$$E_\lambda^{(\pm)} = \bar{E} + \mu^{(\pm)} = \frac{1}{2}(E_1+E_2) \pm \frac{1}{2}\Delta E_\lambda\,, \tag{53}$$

with

$$\Delta E_\lambda = E_\lambda^{(+)} - E_\lambda^{(-)} = \sqrt{(E_1-E_2)^2 + 4\lambda^2|a|^2}\,. \tag{54}$$

We sketch these energy levels $E^{(\pm)}$ in the RH panel of Fig. 2 and compare with the free case ($\lambda \to 0$), dashed lines. We see that for $\lambda \neq 0$ then we have the phenomenon of avoided energy levels for $E_\lambda^{(\pm)}$.

The eigenvectors $e_r^{(\pm)}$ are given by

$$e_r^{(\pm)} = \frac{1}{\sqrt{\Delta E_\lambda}} \begin{pmatrix} \sqrt{\kappa_\pm} \\ \pm \mathrm{sgn}(\lambda)\sqrt{\kappa_\mp}\,\frac{a}{|a|} \end{pmatrix}_r\,, \quad \text{with} \quad \kappa_\pm = \frac{1}{2}\Delta E_\lambda \pm \frac{1}{2}(E_1-E_2)\,, \tag{55}$$

where the normalisation factor has been chosen so that $|e_1^{(\pm)}|^2 + |e_2^{(\pm)}|^2 = 1$. A useful relation is $\kappa_+\kappa_- = \lambda^2|a|^2$. Note that the components of the eigenvectors are related: $e_2^{(-)} = -\mathrm{sgn}(\lambda)a/|a|\, e_1^{(+)}$ and $e_2^{(+)} = \mathrm{sgn}(\lambda)a/|a|\, e_1^{(-)}$. We also see that while the Feynman–Hellmann approach cannot yield any information on the phase of the matrix element from the energy as it is the modulus, the phase is however contained in the eigenvectors as $a = |a|\zeta_a$ (with $\zeta_a = \pm 1, \pm i$ related to the operator being studied).

This result of course includes the degenerate case when the nucleon $\vec{p}$, $\vec{q}$ momenta are arranged so that their energies are the same, $E_2 = E_1$ (the crossing point in the LH panel of Fig. 2. As discussed earlier, this requires the geometry of the $\vec{p}$ and $\vec{q}$ momenta to be chosen such that $\vec{q}^{\,2} = -2\vec{p}\cdot\vec{q}$ with a possible solution $\vec{p} = -\vec{q}/2$. In this case $\Delta E_\lambda = 2|\lambda||a|$ and eigenvectors $\vec{e}^{(\pm)} = (1, \pm\mathrm{sgn}(\lambda)a/|a|)/\sqrt{2}$.

Including the spin index, for the numerical case under consideration in section 5 where we set $\Gamma = \Gamma^{\mathrm{unpol}}$ is to simply average over the spins of the matrix element, $a \to (a_{++} + a_{--})/2$ as given in eq. (45). Relations between a_{--} and a_{++} are given in Appendix A (together with Appendix B).

4.2 Flavour off-diagonal (transition) matrix elements

We shall now consider flavour off-diagonal, or transition, matrix elements taking for definiteness the $\Sigma^- \to n$ decay, or in the isospin limit considered here $\Sigma(sdd) \to N(udd)$ as our example, i.e. an $s \to u$ decay. We take the quark content of the operator as

$$O(\vec{x}) \sim (\bar{u}\gamma s)(\vec{x})\,, \tag{56}$$

thus the action is no longer diagonal in quark flavour space. Let us consider the $|\Sigma\rangle$ and $|N\rangle$ as having nearly-degenerate energies (or quasi-degenerate energies) and apply the previous formalism, in particular eqs. (28) and (29).

Following the discussion in section 4.1, let us consider again $E_\Sigma(\vec{p}) \approx E_N(\vec{p}+\vec{q})$ the parallel case to that of the LH panel of Fig. 2 but now extended to the Σ particle. In the LH panel of Fig. 3 we sketch this situation for the 1-dimensional example. As before we need to be in a region well separated from other degeneracies. We now set

$$|B_1(\vec{p}_1)\rangle = |\Sigma(\vec{p})\rangle\,, \qquad |B_2(\vec{p}_2)\rangle = |N(\vec{p}+\vec{q})\rangle\,. \tag{57}$$

Again from eq. (10) let us write $E_{B_1}(\vec{p}_1) = E_\Sigma(\vec{p}) = \bar{E} + \epsilon_1$ and $E_{B_2}(\vec{p}_2) = E_N(\vec{p}+\vec{q}) = \bar{E} + \epsilon_2$. We then find that $\langle B_r(\vec{p}_r)|\hat{\bar{\mathcal{O}}}(\vec{q})|B_s(\vec{p}_s)\rangle$ has the same structure as in eq. (50). So the results from section 4.1 from eq. (50) – eq. (55) remain unchanged. In the RH panel of Fig. 3, we show the interacting (i.e. $\lambda \neq 0$) case from eq. (53). Again we now have an avoided level crossing. In comparison to the previous case, Fig. 2, while very similar, the degeneracy is now shifted to a slightly smaller momentum value.

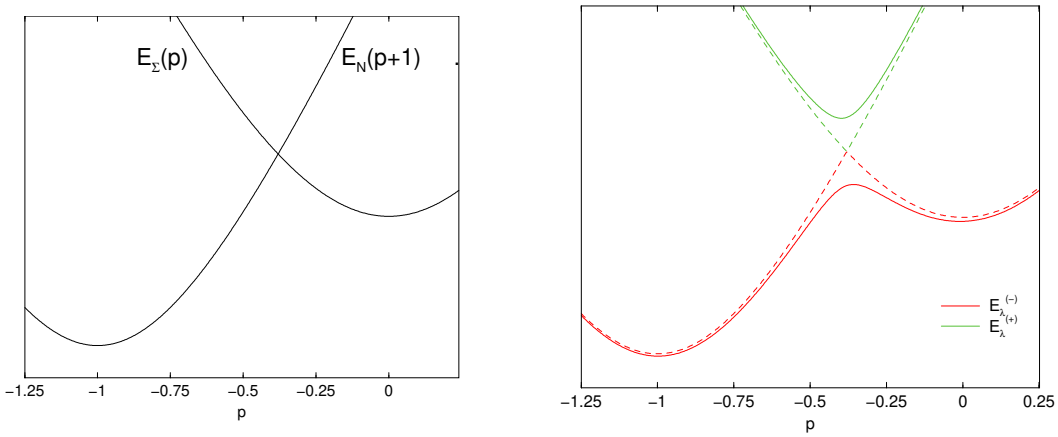

Figure 3: LH panel: A sketch of the (unperturbed) energy states $E_\Sigma(p)$, $E_N(p+q)$ versus p in one dimension for fixed q using units where $q = 1$. RH panel: An equivalent sketch of the perturbed energy states, $E^{(\pm)}$. The dashed lines are the free case. The sketch shows the avoided energy levels.

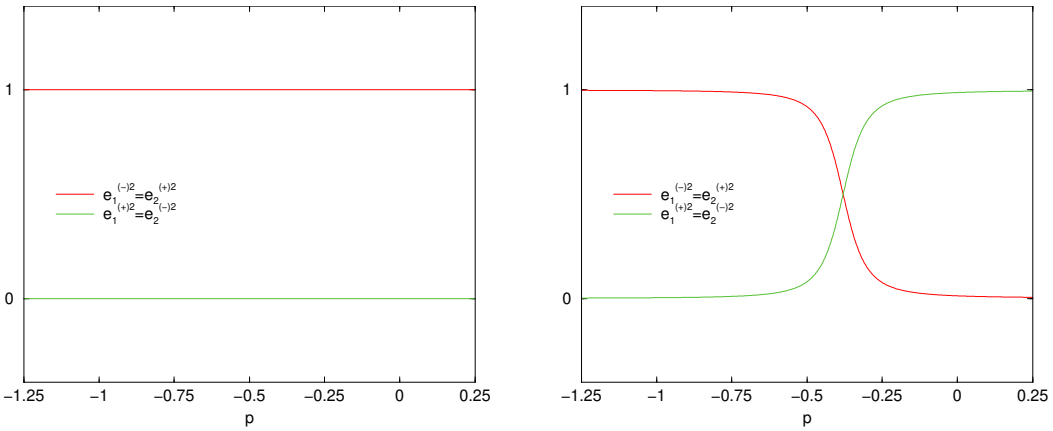

Figure 4: Left panel: The free case where we have plotted $e_1^{(-)\,2}$ and $e_2^{(-)\,2}$ against p, again taking units where $q = 1$. Right panel: The interacting case showing the change of state.

In Fig. 4 we sketch the corresponding eigenvectors to the eigenvalues of Fig. 3. Shown are $e_1^{(-)\,2}$ and $e_2^{(-)\,2}$ against p both for the free and interacting case. While in the free case the components of $\vec{e}^{(\pm)}$ remain constant (left panel) for the interacting case (right panel) they flip as the momentum p changes.

5 A lattice application for transition matrix elements

As an example of this formalism, we shall now consider in more detail how the previous results can be applied to the $\Sigma \to N$ transition matrix element, i.e.

decay $s \to u$ in the isospin limit as described in section 4.2. We first discuss in general the modifications to the action and the fermion inversion procedure before considering the specific numerical results.

5.1 The fermion inversion and correlation functions

To apply the results of section 4.2 we need to consider the action

$$S = S_g + \int_x (\bar{u}, \bar{s}) \begin{pmatrix} D_u & -\lambda\mathcal{T} \\ -\lambda\mathcal{T}' & D_s \end{pmatrix} \begin{pmatrix} u \\ s \end{pmatrix} + \int_x \bar{d}\, D_d\, d\,, \tag{58}$$

where S_g is the gluon action and we shall now consider the fermionic piece in more detail. For simplicity we absorb any clover terms into the Ds. We take the u and d quarks as mass degenerate $m_u = m_d \equiv m_l$, with a common mass m_l. (A more general situation would require a 3×3 matrix, when the vector for u and s would be extended to (u, d, s) with non-degenerate quark masses.) For $\mathcal{T}$ we take the general local expression

$$\mathcal{T}(x, y; \vec{q}) = \gamma\, e^{i\vec{q}\cdot\vec{x}}\, \delta_{x,y}\,. \tag{59}$$

For γ_5-hermiticity for the matrix in eq. (58) we need $\mathcal{T}' = \gamma_5 \mathcal{T}^\dagger \gamma_5$. From the action in eq. (58) we now define the larger flavour inverse propagator, $\mathcal{M}$, as

$$\mathcal{M} = \begin{pmatrix} D_u & -\lambda\mathcal{T} \\ -\lambda\gamma_5\mathcal{T}^\dagger\gamma_5 & D_s \end{pmatrix} \equiv \begin{pmatrix} \mathcal{M}_{uu} & \mathcal{M}_{us} \\ \mathcal{M}_{su} & \mathcal{M}_{ss} \end{pmatrix}, \tag{60}$$

together with $\mathcal{M}_{dd} \equiv D_d$.

We can generate correlation functions, $C_{\lambda rs}(t)$[7] for a fixed $\vec{p}$, $\vec{q}$ by choosing B' and B to be either B_r or B_s, as given in eq. (57). The correlation function matrix for a particular $\vec{p}$, $\vec{q}$ pair and suitable for a GEVP type procedure is thus given by

$$C_{\lambda rs}(t) = \begin{pmatrix} C_{\lambda\Sigma\Sigma}(t) & C_{\lambda\Sigma N}(t) \\ C_{\lambda N\Sigma}(t) & C_{\lambda NN}(t) \end{pmatrix}_{rs}, \tag{61}$$

(see Appendix D for more details). The individual correlation functions in this equation are built from Green's functions given by

$$\begin{pmatrix} G_{uu} & G_{us} \\ G_{su} & G_{ss} \end{pmatrix} = \begin{pmatrix} (\mathcal{M}^{-1})_{uu} & (\mathcal{M}^{-1})_{us} \\ (\mathcal{M}^{-1})_{su} & (\mathcal{M}^{-1})_{ss} \end{pmatrix}. \tag{62}$$

The relations are standard between the correlation functions and Green's functions, for completeness we give them in Appendix D.

[7] While we could consider this as a $(2\times4) \times (2\times4)$ matrix, as in eq. (43), we have projected each correlation function with Γ.

We now need to invert the matrix $\mathcal{M}$ in eq. (60). One possibility is to consider a fermion matrix twice the size to the standard single-flavour fermion matrix for the two flavours. Instead we shall consider here $\mathcal{M}$ as a 2×2 block matrix and invert that. This leads to

$$\begin{aligned} G^{(uu)} &= (1 - \lambda^2 D_u^{-1} \mathcal{T} D_s^{-1} \gamma_5 \mathcal{T}^\dagger \gamma_5)^{-1} D_u^{-1} , \\ G^{(ss)} &= (1 - \lambda^2 D_s^{-1} \gamma_5 \mathcal{T}^\dagger \gamma_5 D_u^{-1} \mathcal{T})^{-1} D_s^{-1} , \end{aligned} \tag{63}$$

and

$$\begin{aligned} G^{(us)} &= \lambda D_u^{-1} \mathcal{T} G^{(ss)} , \\ G^{(su)} &= \lambda D_s^{-1} \gamma_5 \mathcal{T}^\dagger \gamma_5 G^{(uu)} . \end{aligned} \tag{64}$$

The problem with eq. (63) is that it involves an inversion within an inversion, which computationally would be very expensive. However for λ small (the case considered here) it is sufficient to expand to a low order in λ, especially as the expansion parameter is λ^2. Thus given $G_{2n}^{(uu)}$, $G_{2n}^{(ss)}$ we have

$$\begin{aligned} G_{2n+2}^{(uu)} &= D_u^{-1} + \lambda^2 D_u^{-1} \mathcal{T} D_s^{-1} \gamma_5 \mathcal{T}^\dagger \gamma_5 G_{2n}^{(uu)} , \\ G_{2n+2}^{(ss)} &= D_s^{-1} + \lambda^2 D_s^{-1} \gamma_5 \mathcal{T}^\dagger \gamma D_u^{-1} \mathcal{T} G_{2n}^{(ss)} , \end{aligned} \tag{65}$$

for $n = 0, 1, 2, \ldots$, the exact result being obtained for $n \to \infty$. $G_{2n+1}^{(us)}$ and $G_{2n+1}^{(su)}$ for $n = 0, 1, 2, \ldots$ are then given from eq. (64) again using $G_{2n}^{(uu)}$, $G_{2n}^{(ss)}$ as input. Effectively each matrix inversion (either D_u^{-1} or D_s^{-1}) is associated with an additional power of λ. Even powers of λ vanish for transition terms (and correspondingly odd powers of λ vanish for the flavour-diagonal terms). Some more details are given in Appendix E. For example the leading order result ($n = 0$) for both the diagonal and off-diagonal Green's functions are given by

$$\begin{aligned} G^{(uu)} &= D_u^{-1} + O(\lambda^2) , \\ G^{(ss)} &= D_s^{-1} + O(\lambda^2) , \\ G^{(us)} &= \lambda D_u^{-1} \mathcal{T} D_s^{-1} + O(\lambda^3) , \\ G^{(su)} &= \lambda D_s^{-1} \gamma_5 \mathcal{T}^\dagger \gamma_5 D_u^{-1} + O(\lambda^3) , \end{aligned} \tag{66}$$

which is possibly sufficient as there are no $O(\lambda^2)$ terms so the validity of the linear term in λ could extend further. The off-diagonal correlation functions are now just like the usual 3-point function integrated over the insertion time.

To better justify the Feynman–Hellmann procedure, we shall consider higher order iterations to approximate the Green's functions to within numerical accuracy. To build the Green's functions we use $\delta_{\vec{x},\vec{0}} \delta_{t,0}$ as the initial source, and build the chain using the previously calculated object as the new source as given in eq. (65). This has the advantage of producing the Green's function and hence correlation function as a continuous function of λ rather than needing a separate

evaluation for each value of λ chosen. Each subsequent insertion of the operator on the correlation function is constructed using a sequential source with the insertion time being summed over.

Note that for each different operator and momentum $\vec{q}$ we have to re-calculate everything. This is opposite to the usual common procedure for three-point functions, where we calculate the second Green's function from the sink to the operator (which allows many operators to be inserted for one second inversion).

5.2 The simulation

5.2.1 The decay matrix element and chosen kinematics

We shall consider in this article the vector matrix element V_4 for $\Sigma \to N$ where the Σ is stationary, i.e. $\vec{p} = \vec{0}$ (and $\vec{q} = \vec{p}\,' - \vec{0}$). Then the (Euclidean) momentum transfer is given in this case by[8]

$$q = (i(M_\Sigma - E_N(\vec{q})), \vec{q}\,), \quad \text{or} \quad Q^2 = -(M_\Sigma - E_N(\vec{q}))^2 + \vec{q}^{\,2}\,. \tag{67}$$

From eq. (45) we must average the matrix element over the spin index. These can be computed using the results given in Appendix A together with those in Appendix B. This gives[9]

$$\begin{aligned} &\langle N(\vec{q},+)|\bar{u}\gamma_4 s|\Sigma(\vec{0},+)\rangle_{\text{rel}} \\ &= \sqrt{2M_\Sigma(E_N(\vec{q})+M_N)} \\ &\quad \times \left(f_1^{\Sigma N}(Q^2) + \frac{E_N(\vec{q})-M_N}{M_N+M_\Sigma} f_2^{\Sigma N}(Q^2) + \frac{E_N(\vec{q})-M_\Sigma}{M_N+M_\Sigma} f_3^{\Sigma N}(Q^2) \right). \end{aligned} \tag{68}$$

This uses the relativistic normalisation, see eq. (15). (We emphasise this here with the subscript.) Note that the matrix element in eq. (68) can be considered as a function of Q^2 as eq. (67) gives $E_N(\vec{q}) = (Q^2 + M_\Sigma^2 + M_N^2)/(2M_\Sigma)$ which can be used to eliminate $E_N(\vec{q})$ on the RHS of eq. (68). Denoting the various spin components by $a_{\pm\pm}$ then we also find as expected $a_{--} = a_{++}$, $a_{+-} = 0 = a_{-+}$. (For this case, the matrix element is real.) In the following for simplicity we will supress the spin index.

ΔE_λ from eq. (54) is given as the (positive) difference in the perturbed energies

$$\Delta E_\lambda = \sqrt{(M_\Sigma - E_N(\vec{q}))^2 + 4\lambda^2 \left(\frac{\langle N(\vec{q})|\bar{u}\gamma_4 s|\Sigma(\vec{0})\rangle_{\text{rel}}}{(2E_N(\vec{q}))(2M_\Sigma)} \right)^2}. \tag{69}$$

[8] Note that we have adopted the convention that q is positive for a scattering process where for the scattered baryon the momentum q is added to the initial baryon momentum. This is opposite to the semi-leptonic case, where the lepton and neutrino carry momentum q. This was reflected in the choice in section 4.2. While here this convention does not matter, when unified SU(3) flavour breaking expansions are considered, [35], one specific q convention has to be chosen for all cases.

[9] For simplicity we simply write $\hat{O}(\vec{0}) \to \bar{u}\gamma_4 s$.

It is thus sufficient to construct just a matrix of correlation functions, as given in eq. (61) and then apply the GEVP procedure to this.

5.2.2 GEVP

We apply the GEVP (Generalised Eigen-Value Problem) to the 2×2 correlator matrix $C_\lambda(t)$, eq. (61). The variation of the method we use here [24] is to first determine the left $v^{(i)}$ and right $u^{(i)}$ eigenvectors and then project out the eigenvalues

$$c^{(i)}(t) = e^{-E_\lambda^{(i)} t}\,, \tag{70}$$

for $E_\lambda^{(i)}$, $i = \pm$ (see eq. (53)). To achieve this, we consider t_0 and a further time $t_0 + \Delta t_0$ to construct the following eigenvalue equations

$$\begin{aligned} C_\lambda^{-1}(t_0) C_\lambda(t_0 + \Delta t_0) u^{(i)}(t_0, \Delta t_0) &= c^{(i)}(\Delta t_0) u^{(i)}(t_0, \Delta t_0)\,, \\ v^{(i)\dagger}(t_0, \Delta t_0) C_\lambda(t_0 + \Delta t_0) C_\lambda^{-1}(t_0) &= c^{(i)}(\Delta t_0) v^{(i)\dagger}(t_0, \Delta t_0)\,, \quad i = \pm\,. \end{aligned} \tag{71}$$

Solving these equations will give the fixed eigenvectors u and v (i.e. independent of t) which can be combined with the correlator matrix to construct a new correlation function

$$C_\lambda^{(i)}(t) = v^{(i)\,\dagger} C_\lambda(t) u^{(i)}\,, \quad i = \pm\,, \tag{72}$$

which projects out the eigenvalue $c^{(i)}(t)$, eq. (70). Using eqs. (46), (47) this means that

$$v_r^{(i)} = \frac{N^{(i)}}{Z_r}\, e_r^{(i)}\,, \quad \text{and} \quad u_s^{(i)} = \frac{\bar{N}^{(i)}}{\bar{Z}_s}\, e_s^{(i)}\,, \tag{73}$$

where $N^{(i)}$ and $\bar{N}^{(i)}$ are normalisation constants. Essentially $v_r^{(i)*}$ measures the component of B_r in the i^{th} eigenvector and similarly for $u_s^{(i)}$ and $\bar{B}_s$. (The above statements and equations are not restricted to just the $d_s = 2$ case.)

These two correlators $C_\lambda^{(i)}(t)$, $i = \pm$ represent the two low-lying eigenstates of the system which of course includes the perturbation to the action. To relate this to the transition form factors in eq. (69) we thus require the energy splitting between these two states. To extract this energy splitting we construct the ratio of the correlators

$$R_\lambda(t) = \frac{C_\lambda^{(+)}(t)}{C_\lambda^{(-)}(t)} \overset{t \gg 0}{\propto} e^{-\Delta E_\lambda t}\,, \tag{74}$$

which in the large Euclidean time limit will behave like a single exponential function and will show up in the effective energy as a plateau region. We thus use this effective energy to pick out a suitable plateau region and then fit a one-exponential function to the ratio. The two important parameters of the GEVP calculation are t_0 and Δt_0. Optimally the time range from t_0 and $t_0 + \Delta t_0$ needs to be in a region where the ground state is saturated but the signal-to-noise ratio is still sufficiently high to exclude any effects from higher states.

5.2.3 Lattice details

Numerical simulations have been performed using $N_f = 2+1$ $O(a)$ improved clover Wilson fermions [36] at $\beta = 5.50$ and $(\kappa_l, \kappa_s) = (0.121040, 0.120620)$ on a $N_s^3 \times N_t = 32^3 \times 64$ lattice size. More definitions and details are given in [37]. We briefly mention here that our strategy is to keep the average bare quark mass constant from a value on the $SU(3)$ flavour symmetry line. The above (κ_l, κ_s) have been chosen to correspond to $\kappa_l = \kappa_s \equiv \kappa_0 = 0.120900$ at the $SU(3)$ flavour symmetric point. The 'distance' in lattice units from the flavour symmetric line is given by δm_l which is defined by

$$\delta m_l = \frac{1}{2}\left(\frac{1}{\kappa_l} - \frac{1}{\kappa_0}\right), \tag{75}$$

and here is ~ -0.005. $SU(3)$ flavour breaking terms have been determined, which allows an extrapolation to the physical point for both hadron masses, [37] and matrix elements [35, 28]. This situation corresponds to a lattice spacing of $a \sim 0.074\,\mathrm{fm} \sim 1/(2.67\,\mathrm{GeV})$ leading to a pion mass of $\sim 330\,\mathrm{MeV}$. Errors given in the following are primarily statistical (using $\sim O(500)$ configurations) using a bootstrap method.

5.2.4 Twisted boundary conditions

While the formalism developed here is designed to allow non-degenerate energy states (quasi-degenerate energy states), it is clearly necessary to keep the energy of the states close to each other. Spatial momentum on the lattice is discretised and given in each direction in steps of $2\pi/N_s$, which is coarse on this lattice size and makes this requirement difficult to achieve. To obtain a finer energy level separation we use twisted boundary conditions, [38], it being sufficient to apply this just to the valence quarks, [39, 40, 41, 42]. In general we take for a quark, q,

$$q(\vec{x} + N_s\vec{e}_i, t) = e^{i\theta_i} q(\vec{x}, t)\,, \quad i = 1, 2, 3\,. \tag{76}$$

This is rather similar to the Feynman–Hellmann procedure described earlier, and leads to a shift in the momentum in the Green's function by $\vec{\theta}/N_s$. Specifically we choose to compose $\vec{q}$ as a twist for the u quark in the 2-direction. In other words we set the lattice momenta to

$$\vec{p} = \vec{0}\,, \qquad \vec{q} = \left(0, \frac{\theta_2}{N_s}, 0\right), \tag{77}$$

and use the results of section 4.2. For the runs and number of configurations used in this article, we have determined the masses (in lattice units) as $M_N = 0.424(11)$ and $M_\Sigma = 0.461(10)$ close to those given in [37] (the number of configurations used in this study is somewhat smaller). In Table 1 we give the θ_2-parameter values that we have used in our investigation. Run #1 in the table corresponds

run #	θ_2/π	$\vec{q}^2$	E_N	$M_\Sigma - E_N$
1	0.0	0.0	0.424(11)	0.0366(33)
2	0.448	0.0019	0.429(10)	0.0351(35)
3	1	0.0096	0.437(10)	0.0301(42)
4	1.6	0.0247	0.450(12)	0.0182(57)
5	2.06	0.0408	0.462(12)	0.0030(69)
6	2.25	0.0488	0.469(13)	-0.0037(78)

Table 1: θ_2-twist values, together with $\vec{q}^2$, $E_N(\vec{q})$, $M_\Sigma - E_N(\vec{q})$ in lattice units. In addition $M_N = 0.424(11)$ and $M_\Sigma = 0.461(11)$.

to $\vec{q} = \vec{0}$ or "$q_{\max}$", run #2 corresponds approximately to $Q^2 = 0$, while runs #5, #6 are the closest we have achieved to $E_N(\vec{0}+\vec{q}) = E_\Sigma(\vec{0}) = M_\Sigma$. In the table we also give $\vec{q}^2$, $E_N(\vec{q})$ and the difference $M_\Sigma - E_N(\vec{q})$ (all in lattice units). These are the measured values from the relevant 2-point correlation functions.

5.3 Tests

5.3.1 Correlators and GEVP

We first wish to determine the value of n required for the expansions in eq. (65) to provide a good approximation for the full Green's function of eq. (63). In Fig. 5 values of the four correlators for $t_0 = 6$ and $\Delta t_0 = 4$ where the Green's functions and hence correlation functions are computed to various orders of λ by iterating eq. (65)[10]. The LH panel shows the $C_{\lambda\Sigma\Sigma}$ and $C_{\lambda\Sigma N}$ correlation functions with $\lambda = 0.025$. The lower sub-plot shows the ratio of the correlation functions between the two highest orders of λ available, to give an impression of the convergence of the series. For the diagonal correlators we see that the change is negligible, while for the off-diagonal correlation functions the change is at most a few % and in the region where the fits are made (see the following Fig. 6) at most $\sim 1\%$. The RH panel shows the $C_{\lambda NN}$ and $C_{\lambda N\Sigma}$ correlators also at $\lambda = 0.025$. A similar discussion and conclusion holds as for the LH panel.

Applying the GEVP to the 2×2 matrix of correlation functions ΔE_λ is calculated from eq. (74). The results for ΔE_λ are dependent on λ, eq. (69), so as λ increases, the resulting correlation functions will have increasing linear-in-time contributions that become dominant. In Fig. 6 we investigate this by showing the energy difference $(\Delta E_\lambda)_{\text{eff}}$ versus t where using eq. (74) we have $(\Delta E_\lambda)_{\text{eff}} = -\ln(R_\lambda(t+1)/R_\lambda(t))$. Again in the upper two plots the various orders in λ are shown: $O(\lambda)$, $O(\lambda^2)$, $O(\lambda^3)$ and $O(\lambda^4)$. The upper LH panel is with

[10] By this we mean that at any order we include the appropriate lower orders, so for example $O(\lambda^4)$ means we generate the $O(\lambda^0)+O(\lambda^2)+O(\lambda^4)$ terms iterating eq. (65) for the diagonal Green's functions.

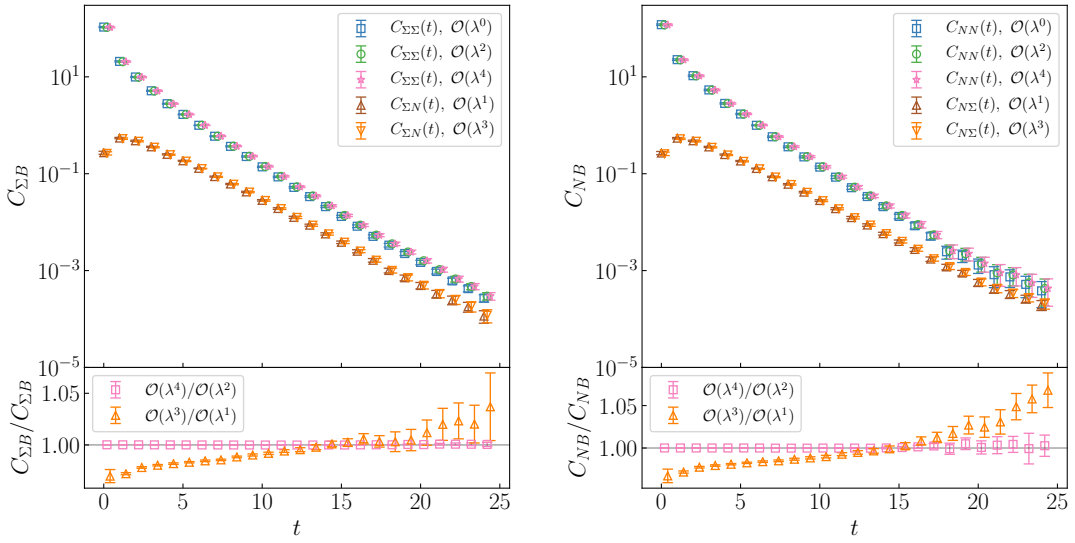

Figure 5: LH panel: The $C_{\lambda\,\Sigma\Sigma}$ correlation functions (at $O(1)$, $O(\lambda^2)$ and $O(\lambda^4)$, squares, circles and stars respectively) and $C_{\lambda\,\Sigma N}$ correlation functions (at $O(\lambda)$ and $O(\lambda^3)$, upper triangles and lower triangles respectively) at $\lambda = 0.025$ against t for $t_0 = 6$ and $\Delta t_0 = 4$. The lower sub-plot shows the ratio of correlation functions $C_{\lambda\,\Sigma B}$ ($B = \Sigma$, squares and $B = N$, triangles) between the two highest orders of λ available. RH panel: Similarly for $C_{\lambda\,NN}$ and $C_{\lambda\,N\Sigma}$. The points are slightly offset for visibility. Both results are for run #5.

$\lambda = 0.025$, while the upper RH panel is for $\lambda = 0.05$. It can be seen that the correlator at $O(\lambda)$ starts to drift up at the higher value of λ, however ΔE_λ for $O(\lambda^4)$ still shows a plateau for this value of λ. Again, as discussed previously for the correlation functions in Fig. 5 this gives an impression of the convergence of the Green's functions in eq. (65) and it's effect on the determined energies. In the lower two plots we use an expanded scale for the $O(\lambda^4)$ results.

We need to check that the parameters used in the GEVP are appropriate and give reliable results. This becomes more of an issue as the energies of the two states come closer together. We will use some criteria to determine an optimal set of parameters [43],

- The correlation functions should have a good statistical signal over the range spanned by t_0 and Δt_0,
- The estimate of the energy difference from $c^{(i)}$ should be close to the final estimate of the energy difference.

The energies can also be estimated directly from the eigenvalues $c^{(i)}$ by using $E_\lambda(c^{(i)}) = -\ln c^{(i)}/\Delta t_0$. Since we are interested in the energy difference between

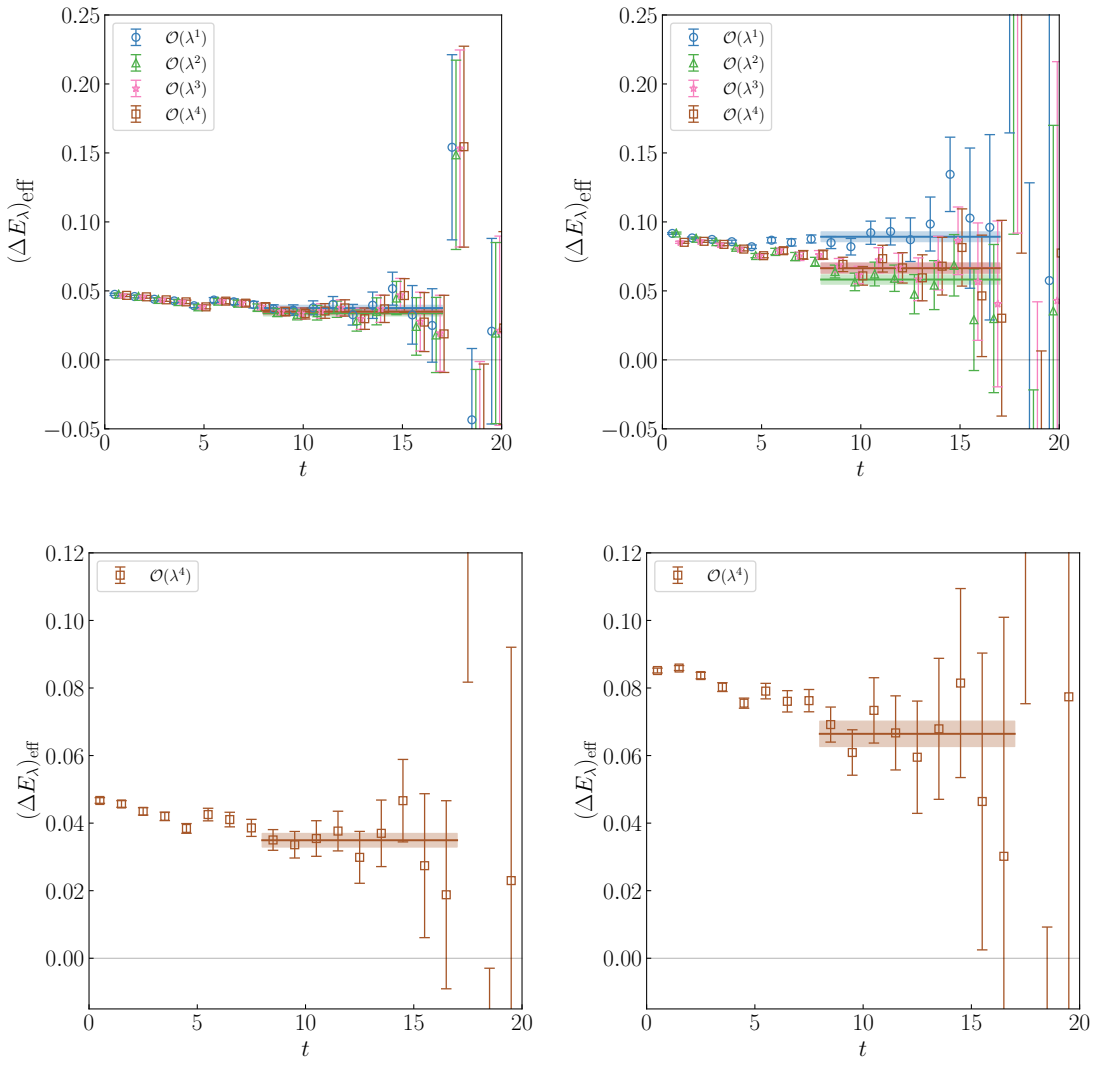

Figure 6: Upper LH panel: $(\Delta E_\lambda)_{\rm eff}$ versus t for $\lambda = 0.025$ at $O(\lambda)$ (circles), $O(\lambda^2)$ (triangles), $O(\lambda^3)$ (stars), $O(\lambda^4)$ (squares) for run #5. Upper RH panel: Similarly for $\lambda = 0.05$. The points are slightly offset for visibility. Also shown is the fit interval used and fit using eq. (74). Lower LH plot: An expanded plot of the upper LH plot at $O(\lambda^4)$ (squares). Lower RH plot: Similarly for the upper RH plot.

the two states, we will consider $\Delta E_\lambda(c^+, c^-) = -\ln(c^{(+)}/c^{(-)})/\Delta t_0$. This alternative estimation will then be compared to the energy shift from fitting to the (diagonal) ratio of correlators as described in eq. (74).

Fig. 7 shows the difference between these two estimates of the energies as a function of both t_0 and Δt_0 for run #5. For $\Delta t_0 \geq 4$ the uncertainty in the difference is reduced and for $t_0 \geq 6$ the difference starts to agree with zero. Therefore we will choose $t_0 = 6$, $\Delta t_0 = 4$ as the parameters for the GEVP in runs #4,

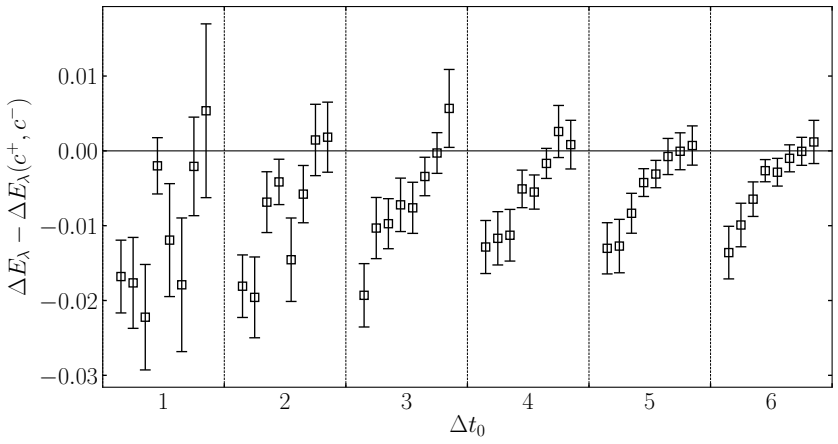

Figure 7: The difference between two estimates of ΔE_λ, one calculated from the eigenvalues of the GEVP and the other from a fit to the ratio of correlators in eq. (74). The difference is shown as a function of both t_0 and Δt_0. For each value of Δt_0 it is shown for the values $t_0 = 1$ – 8, where the dashed lines separate the values of Δt_0. These results are from run #5. The uncertainties are reduced for $\Delta t_0 \geq 4$ and they start agreeing with zero for $t_0 \geq 6$.

#5 and #6. For the first three runs the difference between the energies of the nucleon and Σ is large enough that the GEVP gives consistent results for smaller parameters and so we choose $t_0 = 4$, $\Delta t_0 = 2$ for those runs.

With this preliminary background we now discuss the energy shifts and state mixing.

5.3.2 Energy shifts

We now consider the dependence of ΔE_λ with λ. In Fig. 8 we show the λ dependence for run #1 (left panel) and #5 (right panel). As the numerical results for the correlation functions are coefficients of a polynomial in λ to λ^4 we are able to give the results for ΔE_λ as a continuous function of λ. This allows a comparison of the numerical results for the various orders in λ. Following this we take the range of λ to be determined when the last iteration in λ produces little perceptible numerical effect and we have confidence in the order of approximation of the Green's function in eq. (65). From the plots in Fig. 8 between the $O(\lambda^3)$ and $O(\lambda^4)$ terms this is the case for the range for λ of $0 \leq \lambda \lesssim 0.04$.

5.3.3 State mixing

The eigenvectors which resulted from the GEVP calculation give insight into how much mixing is occuring between the two states at the given λ value. We expect there to be minimal mixing for the data at momentum values which are

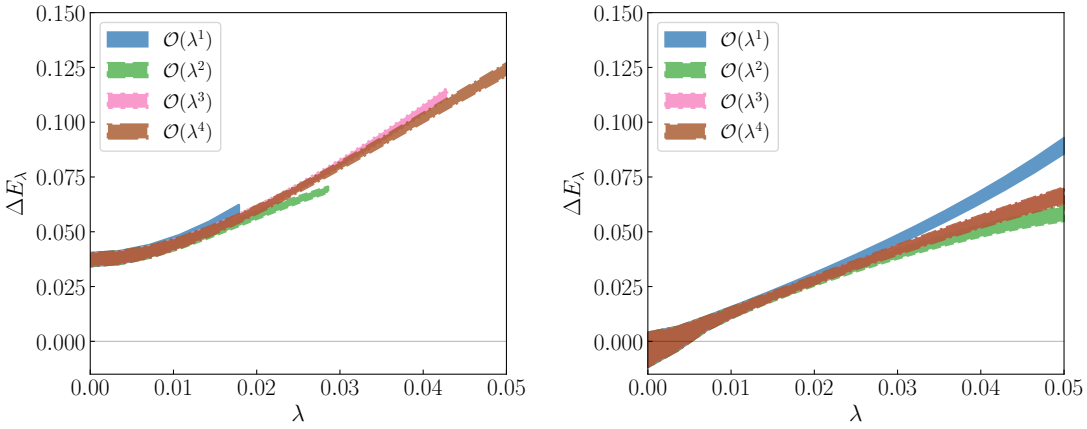

Figure 8: LH panel: The λ-dependence for run #1 for ΔE_λ. The numerical results for each order in λ ($O(\lambda)$, $O(\lambda^2)$, $O(\lambda^3)$ and $O(\lambda^4)$) are given as bands. RH panel: Similarly for run #5.

far removed from the crossover point of the nucleon energy and the sigma mass, and more mixing for momentum values near the crossover point. To show how the mixing changes, we now consider the eigenvectors.

For each eigenvector the square of each component separately will then give an indication of how the mixing changes with respect to the momentum (the normalisation of each eigenvector being 1). This can be seen in Fig. 9 where in the LH panel we plot the normalised $(Z_r v_r^{(-)})^2$ for $r = 1$ (squares) and 2 (triangles) versus $\vec{q}^2$, where $v_r^{(-)}$ is determined by the GEVP procedure. From eq. (73) we see that these are equal to $e_r^{(-)\,2}$. As a check we also show in the RH panel of the figure $e_r^{(-)\,2}$, $r = 1,\ 2$ directly computed from eq. (55) using the previously determined fit values from the energies. (As also discussed there the $e_r^{(+)\,2}$ are related to the $e_r^{(-)\,2}$ by an interchange.) Values near zero or one indicate minimal state mixing and values near 1/2 indicate a high amount of mixing between the states. Mixing occurs after run #4 where $E_N \approx M_\Sigma$.

We shall consider avoided energy level mixing in more detail in the next section, section 6.2.

6 Results

6.1 Energy level comparison

In the RH panel of Fig. 8 it can be seen that it is possible for the energy shift to be negative for small values of λ. This is due to the ordering of the states being difficult to determine at these values of λ. Since the fitting function in eq. (69) is strictly positive, it will not produce a good fit for the runs where ΔE_λ

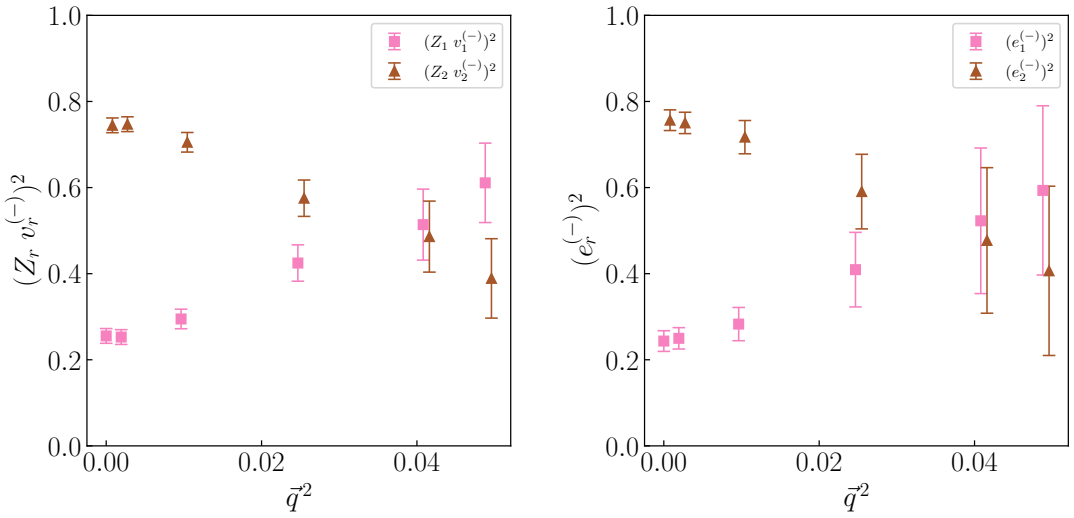

Figure 9: LH panel: Normalised $Z_r v_r^{(-)\,2}$ (r = 1 squares, r = 2 triangles) against $\vec{q}^{\,2}$. From eq. (73) we see that these are equal to $e_r^{(-)\,2}$. RH panel: $e_r^{(-)\,2}$, (r = 1 squares, r = 2 triangles) from eq. (55) against momentum $\vec{q}^{\,2}$. Both plots are for $\lambda = 0.025$.

gets close to zero. To solve this, we square the data and fit to the square of the function in eq. (69). We will also predetermine the value of the energy shift for the unperturbed two-point function $\Delta E_0 = |E_N(\vec{q}) - M_\Sigma|$ (i.e. $\lambda = 0$) and fix this in the fitting function. The matrix element is now the only free parameter.

In Fig. 10 we show the λ dependence of the energy shifts, ΔE_λ, for runs #1 – #6 at $O(\lambda^4)$. These, together with their associated errors, are shown as bands in the figures. A fit is made by using the square of eq. (69). We clearly see in the series of plots that when the quasi-degenerate states become simply degenerate states i.e. if $E_N(\vec{q}) \approx M_\Sigma$ (runs #5, #6) then we have approximate linear behaviour in λ through the origin.

6.2 Avoided energy level crossing

We now investigate avoided energy level crossing. In the LH plot of Fig. 3 we sketched the non-interacting case. In the interacting case (RH plot of Fig. 3) the quasi-energy levels will avoid each other. While previously we only considered ΔE_λ, we now consider each energy level, $E_\lambda^{(\pm)}$, separately. We compute these from eq. (53) by using the previously determined ΔE_λ together with $E_N(\vec{q})$ and M_Σ. In the LH panel of Fig. 11 we plot non-interacting stationary Σ and the measured $E_N(\vec{q})$ against $\vec{q}^{\,2}$ using the $\lambda = 0.025$ results. We see that the energies cross for runs #5 and #6. In the RH panel of Fig. 11 we show the interacting case, where we now see avoided level crossing of the two energy states. This is similar to the case discussed previously in section 4.2.

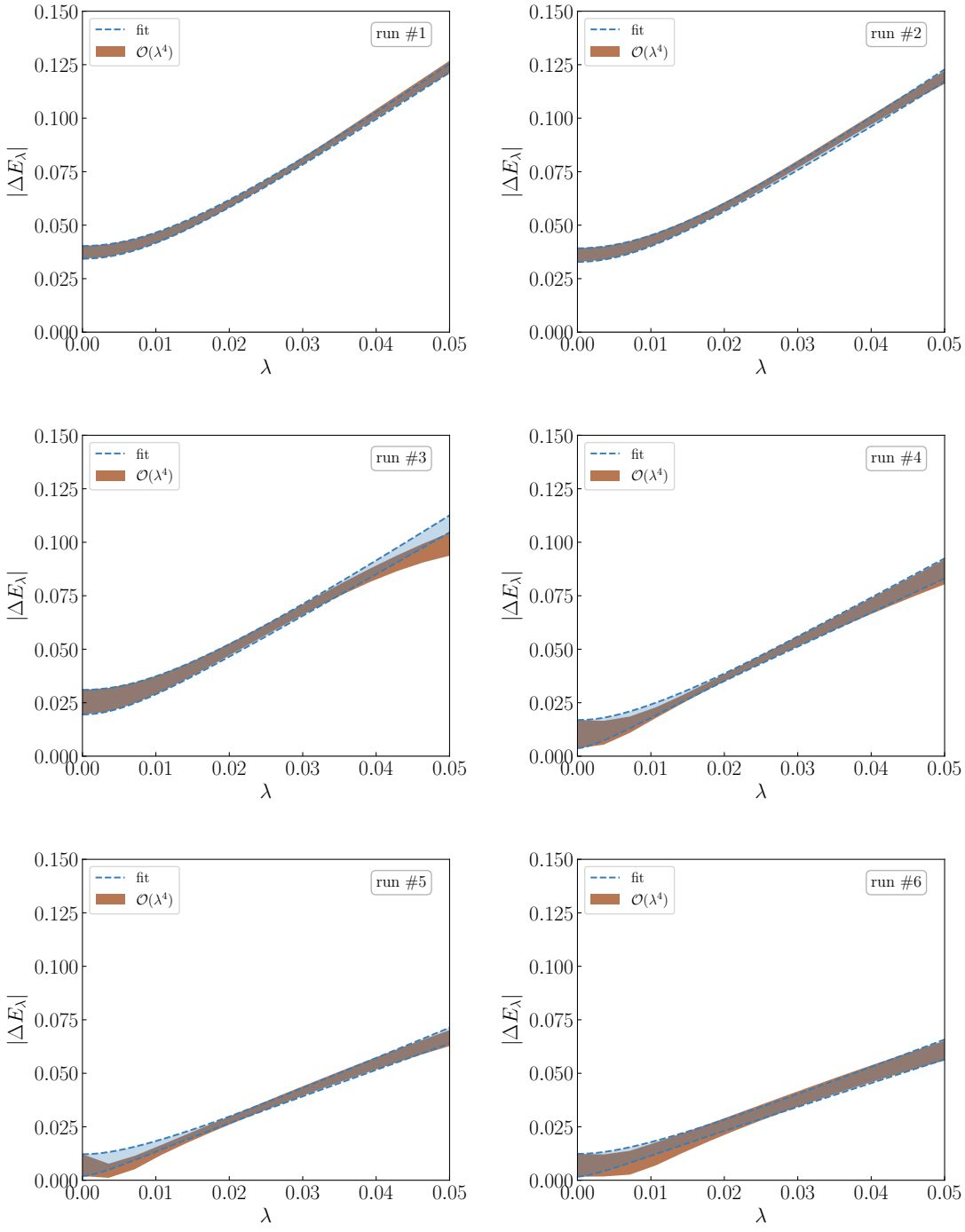

Figure 10: The λ-dependence for runs #1 (top left), #2 (top right), #3 (centre left), #4 (centre right) #5 (bottom left) and #6 (bottom right) for ΔE_λ. The numerical results at $O(\lambda^4)$ are given as bands. The fits are given from using the square of eq. (69) as further discussed in the text.

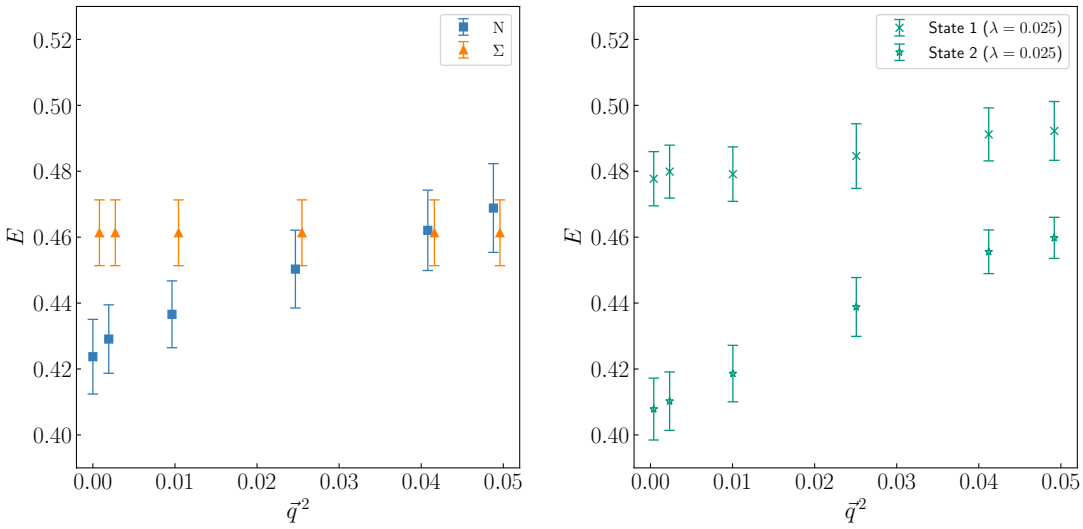

Figure 11: LH panel: The non-interacting Σ mass (filled triangles) and N energy states (filled squares) as a function of $\vec{q}^2$ using the results of Table 1. RH panel: The mixed states $E_\lambda^{(-)}$ shown as crosses and $E_\lambda^{(+)}$ shown as stars.

6.3 Result comparison

The results shown in section 6.1 are for the 'bare' matrix element. We take the renormalisation constant $Z_V = 0.863(4)$, [35]. This is determined from quark-counting for the flavour diagonal matrix elements at zero 3-momentum. Practically this means for this transition matrix element that $f_1^{\Sigma N}$ is renormalised. For from eq. (68) at $\vec{q} = \vec{0}$, the coefficient of the $f_2^{\Sigma N}$ term vanishes, the coefficient of the $f_3^{\Sigma N}$ term is $O(M_\Sigma - M_N) \sim O(\delta m_l)$, while $f_3^{\Sigma N}$ is also $O(\delta m_l)$ and hence this term is $O(\delta m_l)^2$ and so is negligible. (δm_l the 'distance' from the flavour symmetric line is given in eq. (75).) For the matrix element expansions in δm_l see, for example, [35, 28].

We first wish to compare our results with other derivations using the standard approach, e.g. [44], by computing 3-point correlation functions. Briefly, for completeness, defining an (unpolarised) 3-point correlation function

$$C_{NV_4\Sigma}(t,\tau;\vec{q},\vec{0}) = \mathrm{tr}\Gamma^{\mathrm{unpol}}\langle\hat{\bar{N}}(t;\vec{q})\hat{V}_4(\tau)\hat{\bar{\Sigma}}(0,\vec{0})\rangle\,, \tag{78}$$

analogously to the 2-point correlation function of eq. (1) and eq. (43) and applying the same techniques as described earlier and results from section B.2.1 we look

for a plateau in the ratio $R(t,\tau;\vec{0},\vec{p})$ defined as

$$\begin{aligned} R(t,\tau;\vec{q},\vec{0}) &= \frac{C_{NV_4\Sigma}(t,\tau;\vec{q},\vec{0})}{C_{\Sigma\Sigma}(t;\vec{0})}\sqrt{\frac{C_{\Sigma\Sigma}(\tau;\vec{0})C_{\Sigma\Sigma}(t;\vec{0})C_{NN}(t-\tau;\vec{q})}{C_{NN}(\tau;\vec{q})C_{NN}(t;\vec{q})C_{\Sigma\Sigma}(t-\tau;\vec{0})}} \\ &= \frac{1}{\sqrt{2E_N(\vec{q})2M_\Sigma}}\langle N(\vec{q})|\bar{u}\gamma_4 s|\Sigma(\vec{0})\rangle_{\text{rel}}\,. \end{aligned} \tag{79}$$

A similar result holds for $C_{\Sigma V_4^\dagger N}(t,\tau;\vec{0},\vec{q})$ by swapping $\Sigma \leftrightarrow N$ and considering the inverse process. At $\vec{q}=\vec{0}$, the 'double ratio' method, e.g. [41] is employed

$$\begin{aligned} R(t,\tau;\vec{0},\vec{0}) &= \sqrt{\frac{C_{NV_4\Sigma}(t,\tau;\vec{0},\vec{0})C_{\Sigma V_4^\dagger N}(t,\tau;\vec{0},\vec{0})}{C_{\Sigma\Sigma}(t;\vec{0})C_{NN}(t;\vec{0})}} \\ &= \frac{1}{\sqrt{2M_N 2M_\Sigma}}\langle N(\vec{q})|\bar{u}\gamma_4 s|\Sigma(\vec{0})\rangle_{\text{rel}}\,. \end{aligned} \tag{80}$$

For this case this gives reduced error bars and a more prominent plateau.

In Fig. 12 various comparison ratios are shown for $Q^2 \sim 0.27\,\text{GeV}^2$ for the 3-point correlation function approach, using eq. (79). The individual results for a given t (i.e. difference between baryon source and sink times) have smaller error bars, but due to excited states in the 3-point correlation functions we have to perform measurements for various t and extrapolate. An excited state can be accounted for by expanding the 2- and 3-point correlation functions to include contributions from such an excited state and globally fitting for various t values, here $t = 10$, 13 and 16, simultaneously (following for example [49]). The masses (including the excited state masses) have been previously determined from 2-point correlation function. This gives the various fits in Fig. 12. The constant in the fit then gives the relevant matrix element as in eq. (79). Again all calculations are performed on the same set of gauge configurations with 500 configurations used for each source-sink separation.

The Feynman-Hellmann approach has larger error bars, but as a 2-point correlation function measurement we largely avoid this extrapolation. A comparison with the result of run #5 ($Q^2 \sim 0.29\,\text{GeV}^2$) is also given in the figure both for the various t_{sep} and the extrapolated value. The results are compatible for the different approaches.

The results are given in Table 2 and in Fig. 13 we plot $\langle N(\vec{q})|\bar{u}\gamma_4 s|\Sigma(\vec{0})\rangle^{\text{ren}}_{\text{rel}}$ for runs #1 – #6 against Q^2. There is good overall agreement between the two methods and in particular confirm the values obtained from the approach using the Feynman–Hellmann theorem.

These results show that the Feynman-Hellmann theorem can be used for the calculation of transition form factors using two-point functions. This opens the way for more extensive calculations which can make use of the many tools and techniques available for controlling the contamination due to excited states in two-point functions.

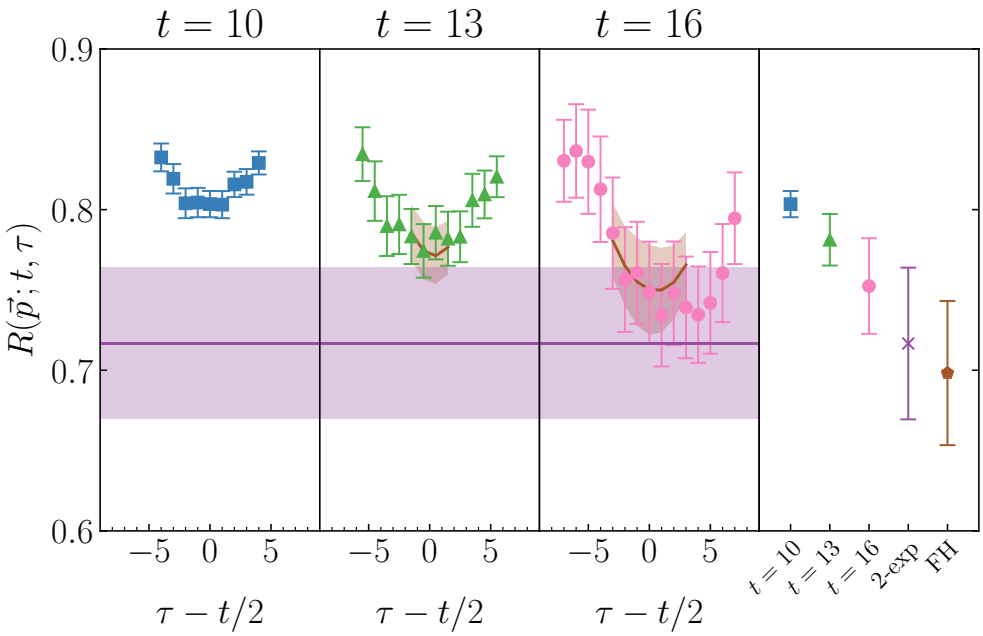

Figure 12: Comparing the three-point correlation function results to the Feynman-Hellmann results. Left to right the first three plots for the three-point function ratios for sink–source separation t = 10, 13 and 16 (filled squares, diamonds and crosses respectively). Global fits including a single additional excited state are also shown. The horizontal band shows the global fit value for the matrix element. The fourth RH plot shows these results for the three t values together with their extrapolated value (cross). For comparison we also show the closest Feynman-Hellmann result, filled upper triangle for run #5.

7 Conclusions

In this article we have extended the use of the Feynman–Hellmann theorem in calculating (nucleon) matrix elements with momentum transfer to situations where the relevant energy levels are not degenerate, but nearly degenerate or quasi-denerate as sketched in Fig. 1. While for flavour-diagonal matrix elements this increases the scope of application of the Feynman–Hellmann theorem, as the associated energy levels now do not have to be exactly degenerate, it now additionally allows for the computation of transition matrix elements. These latter matrix elements are naturally derived using quasi-degenerate energy states.

In section 3, using the Dyson expansion in the Hamiltonian formalism, where the relevant operator is regarded as a perturbation in an expansion parameter λ, see eq. (5), we gave a derivation of the basic result leading to eq. (28). In section 4 several examples are discussed, first for flavour diagonal matrix elements and then followed by flavour off-diagonal or transition matrix elements.

run #	Q^2 [GeV^2]	$\langle N(\vec{q})\|\bar{u}\gamma_4 s\|\Sigma(\vec{0})\rangle^{\rm ren}_{\rm rel}$
1	-0.0095	0.897(27)
2	0.0048	0.878(32)
3	0.062	0.817(40)
4	0.17	0.684(49)
5	0.29	0.535(38)
6	0.35	0.486(42)
a	-0.01	0.883(16)
b	0.21	0.596(37)
c	0.27	0.548(38)
d	0.43	0.397(47)
e	0.52	0.390(51)

Table 2: The renormalised matrix element, $\langle N(\vec{q})|\bar{u}\gamma_4 s|\Sigma(\vec{0})\rangle^{\rm ren}_{\rm rel}$ against Q^2 in GeV^2 for the six runs. We also give five additional Q^2 results: runs $\#a$ – $\#e$ using the methods described in eqs. (78) – (80).

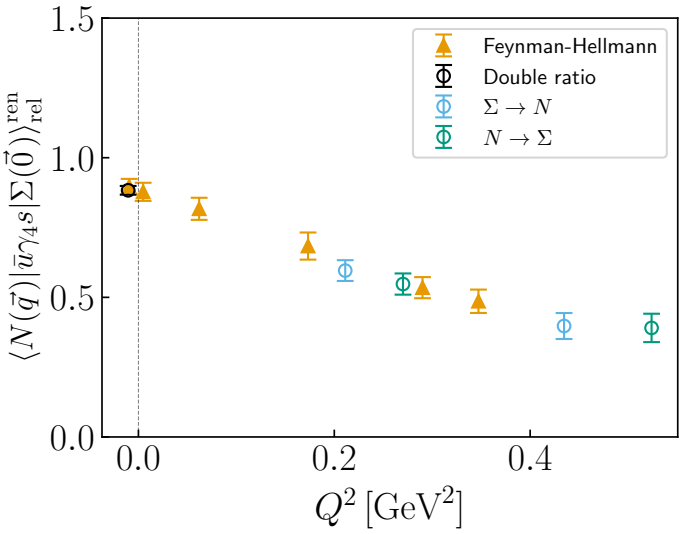

Figure 13: Results for $\langle N(\vec{q})|\bar{u}\gamma_4 s|\Sigma(\vec{0})\rangle^{\rm ren}_{\rm rel}$ versus Q^2. Runs #1 – #6 are given as (filled) triangles. We also make a comparison for this result with results using standard approaches to the computation. The (open) circles are results obtained from the 3-point correlation function, eq. (79) or the double ratio, eq. (80).

An example of the $\Sigma \to N$ decay (i.e. $s \to u$ transition) for the vector current is considered. This necessitates the generalisation of the action to include flavour non-diagonal terms. To minimise numerical cost this is expanded to a sufficiently

high order in λ and then the two-point correlation function is reconstructed allowing a range of λ to be considered. Numerical results are then discussed in section 5. Avoided level crossing is demonstrated for the quasi-degenerate enery states. A comparison is made with results for the matrix element using the conventional 3-point correlation function approach. Although in this article we only consider the vector current transition matrix element, in the Appendices, for completeness, we give the results for all possible Dirac structures of the currents.

The availability of a large range of source-sink separations and the fact that there is only one exponentially decreasing set of excited states to deal with reduces the complexity of this task compared to the equivalent three-point function calculations. Additionally, the expansion of the matrix inversion in terms of the perturbation parameter used in this method presents a convenient way to extend the applicable range of this method. Further calculations will be required to determine whether it remains viable when approaching the physical quark masses when there are larger mass splittings.

Acknowledgements

The numerical configuration generation (using the BQCD lattice QCD program [50])) and data analysis (using the Chroma software library [51]) was carried out on the DiRAC Blue Gene Q and Extreme Scaling (EPCC, Edinburgh, UK) and Data Intensive (Cambridge, UK) services, the GCS supercomputers JUQUEEN and JUWELS (NIC, Jülich, Germany) and resources provided by HLRN (The North-German Supercomputer Alliance), the NCI National Facility in Canberra, Australia (supported by the Australian Commonwealth Government) and the Phoenix HPC service (University of Adelaide). KUC is supported by the ARC grant DP220103098. RH is supported in part by the STFC grant ST/P000630/1. PELR is supported in part by the STFC grant ST/G00062X/1. GS is supported by DFG grant SCHI 179/8-1. RDY and JMZ are supported by the ARC grants DP190100298 and DP220103098. For the purpose of open access, the authors have applied a Creative Commons Attribution (CC BY) licence to any author accepted manuscript version arising from this submission.

Appendix

A Euclidean matrix elements

We take the Minkowski generalised currents to be given by

$$J^F(x) = (\bar{q}F\gamma q)(x) \equiv \sum_{f_1,f_2=1}^{3} F_{f_1,f_2}(\bar{q}_{f_1}\gamma q_{f_2})(x)\,, \tag{81}$$

where q is a flavour vector, $q = (u, d, s)^T$, F is a flavour matrix and with $\gamma = \gamma_\mu$, $\gamma_\mu\gamma_5$, I, $i\gamma_5$, $\sigma_{\mu\nu} = i/2[\gamma_\mu, \gamma_\nu]$ for the vector, axial, scalar, pseudoscalar and tensor currents. (This ensures that $J^{F\,\dagger} = J^{F^T}$.) The further generalisation to operators including covariant derivatives is straightforward. We then take the Minkowski form factors as given in [35].

The Euclidean matrix elements are given by[11]

$$\langle B'(\vec{p}', \sigma')|J^F(\vec{q})|B(\vec{p}, \sigma)\rangle = \bar{u}_{B'}(\vec{p}', \sigma')\mathcal{J}^F(q)u_B(\vec{p}, \sigma)\,, \tag{82}$$

where the generalised currents $J^F(\vec{q})$ [12] also have the same flavour structure as defined by eq. (81) but now using the conventions in [32] with the Euclidean gamma matrices $\gamma = \gamma_\mu$, $i\gamma_\mu\gamma_5$, I, $\gamma_5 = \gamma_1\gamma_2\gamma_3\gamma_4$, $\sigma_{\mu\nu} = i/2[\gamma_\mu, \gamma_\nu]$ for vector V_μ, axial A_μ, scalar, S, pseudoscalar, P, and tensor, $T_{\mu\nu}$, respectively. The Euclidean gamma matrices, γ_μ, are now all Hermitian, $\gamma_\mu^\dagger = \gamma_\mu$. The relation between the Euclidean formulation of the action and Hamiltonian (and hence also for matrix elements) is discussed in [52, 53]. Suppressing the flavour matrix, the $\mathcal{J}^F(q)$ are given by

$$\begin{aligned}
\mathcal{V}_\mu(q) &= \gamma_\mu f_1^{\mathrm{BB}'}(Q^2) + \sigma_{\mu\nu}q_v\frac{f_2^{\mathrm{BB}'}(Q^2)}{M_{B'}+M_B} - iq_\mu\frac{f_3^{\mathrm{BB}'}(Q^2)}{M_{B'}+M_B}\,,\\
\mathcal{A}_\mu(q) &= i\gamma_\mu\gamma_5 g_1^{\mathrm{BB}'}(Q^2) + i\sigma_{\mu\nu}\gamma_5 q_v\frac{g_2^{\mathrm{BB}'}(Q^2)}{M_{B'}+M_B} + q_\mu\gamma_5\frac{g_3^{\mathrm{BB}'}(Q^2)}{M_{B'}+M_B}\,,\\
\mathcal{S}(q) &= g_S^{\mathrm{BB}'}(Q^2)\,,\\
\mathcal{P}(q) &= g_P^{\mathrm{BB}'}(Q^2)\,,\\
\mathcal{T}_{\mu\nu}(q) &= \sigma_{\mu\nu}h_1^{\mathrm{BB}'}(Q^2) + (q_\mu\gamma_\nu - q_\nu\gamma_\mu)\frac{h_2^{\mathrm{BB}'}(Q^2)}{M_{B'}+M_B}\\
&\quad -(\sigma_{\mu\lambda}q_\nu - \sigma_{\nu\lambda}q_\mu)q_\lambda\frac{h_3^{\mathrm{BB}'}(Q^2)}{(M_{B'}+M_B)^2} + 2\epsilon_{\mu\nu\rho\sigma}q_\rho\gamma_\sigma\gamma_5\frac{h_4^{\mathrm{BB}'}(Q^2)}{M_{B'}+M_B}\,.
\end{aligned} \tag{83}$$

As we are using the conventions of [35] then we have taken in these expressions

$$q = p' - p = (i(E_{B'} - E_B), \vec{p}' - \vec{p})\,. \tag{84}$$

This is the convention for scattering processes, rather than the natural convention for decay processes where the opposite holds. However for consistency we remain with the above.

We have also manipulated the tensor results from the expressions given in [35]. For completeness, we briefly describe this here. First to give them in a form as a function of q, only we use a Gordan identity which in Euclidean form is

$$p_\mu \pm p'_\mu = \gamma_\mu\not{p} \pm \not{p}'\gamma_\mu + i\sigma_{\mu\nu}(p_\nu \mp p'_\nu)\,, \tag{85}$$

[11] We use in this Appendix the relativistic normalisation, see eqs. (14) and (15).

[12] Again we are simplifying the notation, from eq. (6) we have $\hat{O}(\vec{x}) \to J^F(\vec{x})$ and $\hat{\tilde{O}}(\vec{q}) \to J^F(\vec{q})$.

together with $\not{p}u = iMu$ and $\bar{u}\not{p} = iM\bar{u}$. This means that h_2 is replaced by $h_2 + h_3$ and there is now a new structure $(\sigma_{\mu\lambda}q_\nu - \sigma_{\nu\lambda}q_\mu)q_\lambda$. Secondly we use the antisymmetric piece of the identity

$$\gamma_\mu\gamma_\rho\gamma_\nu = \gamma_\mu\delta_{\rho\nu} - \gamma_\rho\delta_{\mu\nu} + \gamma_\nu\delta_{\mu\rho} - \epsilon_{\mu\rho\nu\sigma}\gamma_\sigma\gamma_5\,, \tag{86}$$

with $\epsilon_{1234} = +1$ to modify the h_4 structure. Finally for the axial current for the g_2 term we can use

$$\sigma_{\mu\nu}\gamma_5 = -\frac{1}{2}\epsilon_{\mu\nu\rho\lambda}\sigma_{\rho\lambda}\,. \tag{87}$$

With these additional manipulations all the terms in the matrix element decomposition are functions of q and also all the Dirac structure is in the standard gamma-matrix basis.

From the direct computation of the spinor bilinears, as detailed in Appendix B and then using eq. (82) together with eq. (83) we find

$$\begin{aligned}\langle B'(\vec{p}',-)|J^F|B(\vec{p},-)\rangle &= \eta_\gamma\langle B'(\vec{p}',+)|J^F|B(\vec{p},+)\rangle^*\,,\\ \langle B'(\vec{p}',-)|J^F|B(\vec{p},+)\rangle &= -\eta_\gamma\langle B'(\vec{p}',+)|J^F|B(\vec{p},-)\rangle^*\,,\end{aligned} \tag{88}$$

where $\eta_\gamma = \pm$. Explicitly we have the results as given in Table 3. These can be

γ	γ_4	γ_i	$i\gamma_4\gamma_5$	$i\gamma_i\gamma_5$	I	γ_5	σ_{i4}	σ_{ij}	$\sigma_{i4}\gamma_5$	$\sigma_{ij}\gamma_5$
η_γ	+	−	+	−	+	−	+	−	−	+

Table 3: The η_γ factors.

helpful in determining whether the computed matrix element is real or imaginary.

B Spinor bilinear results

The spinor bilinear forms are the most general possible, so to deal with this we shall consider a specific representation – the Dirac representation. Some more general results are given for example in [45, 46, 47, 48]. Again we shall be in Euclidean space.

B.1 General

Sigma matrices

$$\sigma_1 = \begin{pmatrix} 0 & 1 \\ 1 & 0 \end{pmatrix}, \qquad \sigma_2 = \begin{pmatrix} 0 & -i \\ i & 0 \end{pmatrix}, \qquad \sigma_3 = \begin{pmatrix} 1 & 0 \\ 0 & -1 \end{pmatrix}, \tag{89}$$

where

$$\sigma_i\sigma_j = \delta_{ij} + i\epsilon_{ijk}\sigma_k\,, \qquad \sigma_i^\dagger = \sigma_i\,. \tag{90}$$

Gamma matrices

$$\gamma_i = \begin{pmatrix} 0 & -i\sigma_i \\ i\sigma_i & 0 \end{pmatrix}, \qquad \gamma_4 = \begin{pmatrix} 1 & 0 \\ 0 & -1 \end{pmatrix}, \qquad \gamma_5 = \gamma_1\gamma_2\gamma_3\gamma_4 = \begin{pmatrix} 0 & -1 \\ -1 & 0 \end{pmatrix}. \tag{91}$$

B.2 u-spinors

Solving the (free) Dirac equation gives for the $+ve$ energy spinors

$$u(\vec{p},\sigma) = s\begin{pmatrix} \chi^{(\sigma)} \\ \frac{\vec{\sigma}\cdot\vec{p}}{s^2}\,\chi^{(\sigma)} \end{pmatrix}. \tag{92}$$

where it is convenient to define in the following

$$s(\vec{p}) = \sqrt{E(\vec{p}) + M}\,. \tag{93}$$

The spin is quantised along the 3$^{\rm rd}$ direction (due to the nature of the σ_3 matrix in particular) so $\sigma = \pm$ and the 2 component spinors at rest are given by

$$\chi^{(+)} = \begin{pmatrix} 1 \\ 0 \end{pmatrix}, \qquad \chi^{(-)} = \begin{pmatrix} 0 \\ 1 \end{pmatrix}, \tag{94}$$

or in components

$$\chi^{(\sigma)}_{\sigma_r} = \delta_{\sigma\sigma_r}\,, \quad \sigma = \pm\,,\ \sigma_r = \pm\,. \tag{95}$$

We also have

$$\bar{u}(\vec{p},\sigma) = s\left(\chi^{(\sigma)T}\,, -\chi^{(\sigma)T}\,\frac{\vec{\sigma}\cdot\vec{p}}{s^2}\right). \tag{96}$$

As a check we have $\not{p}\,u = iMu$, $\bar{u}\not{p} = iM\bar{u}$ as expected, as the Minkowski free Dirac equation $(\not{p} - m)u = 0$ and upon Euclideanisation $\not{p} \to -i\not{p}$ where p_4 is imaginary.

$\chi^{(\sigma)}$ has the (obvious) property $\chi^{(\sigma')T}\chi^{(\sigma)} = \delta_{\sigma'\sigma}$ which from eqs. (92), (96) gives the standard normalisation of

$$\bar{u}(\vec{p},\sigma')\,u(\vec{p},\sigma) = 2M\,\chi^{(\sigma')T}\chi^{(\sigma)} = 2M\,\delta_{\sigma'\sigma}\,. \tag{97}$$

As $\chi^{(\sigma')}$, $\chi^{(\sigma)}$ just pick out the components of σ_k in $\chi^{(\sigma')T}\sigma_k\chi^{(\sigma)}$ then we have

$$\chi^{(\sigma')T}\sigma_k\chi^{(\sigma)} = (\sigma_k)_{\sigma'\sigma} = \sigma\delta_{k3}\delta_{\sigma'\sigma} + (\delta_{k1} + i\sigma\delta_{k2})\delta_{\sigma',-\sigma}\,, \tag{98}$$

or in vector form

$$(\vec{\sigma})_{\sigma',\sigma} = \sigma\vec{e}_3\,\delta_{\sigma'\sigma} + (\vec{e}_1 + i\sigma\vec{e}_2)\,\delta_{\sigma',-\sigma}\,. \tag{99}$$

In the following we will find

$$\begin{aligned} \bar{u}'(\vec{p}',-)\gamma u(\vec{p},-) &= \eta_\gamma[\bar{u}'(\vec{p}',+)\gamma u(\vec{p},+)]^*\,, \\ \bar{u}'(\vec{p}',-)\gamma u(\vec{p},+) &= -\eta_\gamma[\bar{u}'(\vec{p}',+)\gamma u(\vec{p},-)]^*\,, \end{aligned} \tag{100}$$

where $\eta_\gamma = \pm$. These will be the same factors as given in Table 3.

B.2.1 Bilinears – general case

Vector: γ_4, γ_i

$$\begin{aligned}\bar{u}'(\vec{p}',\cdot)\gamma_4 u(\vec{p},\cdot) &= \left(s's+\frac{\vec{p}'\cdot\vec{p}}{s's}\right)I+\frac{i}{s's}(\vec{p}'\times\vec{p})\cdot\vec{\sigma}\,,\\ \bar{u}'(\vec{p}',\cdot)\gamma_i u(\vec{p},\cdot) &= -i\left(\frac{s'}{s}\vec{p}+\frac{s}{s'}\vec{p}'\right)_i I+\left(\left(\frac{s'}{s}\vec{p}-\frac{s}{s'}\vec{p}'\right)\times\vec{\sigma}\right)_i\,,\end{aligned} \tag{101}$$

where we have suppressed the spin σ index, to have a matrix equation in spin space (e.g. the σ',σ components of $\bar{u}'(\vec{p}',\cdot)\gamma_4 u(\vec{p},\cdot)$ are $\bar{u}'(\vec{p}',\sigma')\gamma_4 u(\vec{p},\sigma)$). The above equation (eq. (101)) is written in a compact form. This can be 'undone' by using eq. (98) (or eq. (99)) for $\vec{\sigma}_{\sigma'\sigma}$. This then allows the spin relation in eq. (100) to be shown with, for this case, $\eta_{\gamma_4}=+$ and $\eta_{\gamma_i}=-$. As expected this result is independent of the kinematic factors $\vec{p}'$ and $\vec{p}$ and just depends on the factors: i, σ and the combination $i\sigma$. The other cases follow a similar pattern.

Axial: $i\gamma_4\gamma_5$, $i\gamma_i\gamma_5$

$$\begin{aligned}\bar{u}'(\vec{p}',\cdot)i\gamma_4\gamma_5 u(\vec{p},\cdot) &= -i\left(\frac{s'}{s}\vec{p}+\frac{s}{s'}\vec{p}'\right)\cdot\vec{\sigma}\,,\\ \bar{u}'(\vec{p}',\cdot)i\gamma_i\gamma_5 u(\vec{p},\cdot) &= \frac{i}{s's}(\vec{p}'\times\vec{p})_i I-\left(s's\delta_{ij}+\frac{1}{s's}(p'_ip_j+p'_jp_i-\vec{p}'\cdot\vec{p}\,\delta_{ij})\right)\sigma_j\,,\end{aligned} \tag{102}$$

with $\eta_{i\gamma_4\gamma_5}=+$ and $\eta_{i\gamma_i\gamma_5}=-$.

Scalar: I

$$\bar{u}'(\vec{p}',\cdot)Iu(\vec{p},\cdot)=\left(s's-\frac{\vec{p}'\cdot\vec{p}}{s's}\right)I-\frac{i}{s's}(\vec{p}'\times\vec{p})\cdot\vec{\sigma}\,, \tag{103}$$

with $\eta_I=+$.

Pseudoscalar: γ_5

$$\bar{u}'(\vec{p}',\cdot)\gamma_5 u(\vec{p},\cdot)=-\left(\frac{s'}{s}\vec{p}-\frac{s}{s'}\vec{p}'\right)\cdot\vec{\sigma}\,, \tag{104}$$

with $\eta_{\gamma_5}=-$.

Tensor:

- $\sigma_{i4}=i\gamma_i\gamma_4$, $\sigma_{ij}=i\gamma_i\gamma_j\ (i\neq j)$

$$\begin{aligned}\bar{u}'(\vec{p}',\cdot)\sigma_{i4}u(\vec{p},\cdot) &= -\left(\frac{s'}{s}\vec{p}-\frac{s}{s'}\vec{p}'\right)_i I-i\left(\left(\frac{s'}{s}\vec{p}+\frac{s}{s'}\vec{p}'\right)\times\vec{\sigma}\right)_i\,,\\ \bar{u}'(\vec{p}',\cdot)\sigma_{ij}u(\vec{p},\cdot) &= -\frac{i}{s's}(p'_ip_j-p'_jp_i)I\\ &\quad+\epsilon_{ijk}\left(-s's\,\delta_{kl}+\frac{1}{s's}\left(p_kp'_l+p'_kp_l-\vec{p}'\cdot\vec{p}\,\delta_{kl}\right)\right)\sigma_l\,,\end{aligned} \tag{105}$$

with $\eta_{\sigma_{i4}} = +$ and $\eta_{\sigma_{ij}} = -$.

- An alternative tensor form for $\sigma_{\mu\nu}\gamma_5$ and using the identity of eq. (87) is

$$\bar{u}'(\vec{p}',\sigma')\sigma_{i4}\gamma_5 u(\vec{p},\sigma) = -\frac{1}{2}\epsilon_{ikl}\,\bar{u}'(\vec{p}',\sigma')\sigma_{kl}u(\vec{p},\sigma)\,, \tag{106}$$

with $\eta_{\sigma_{i4}\gamma_5} = -$. A more explicit expression can then be given using eq. (105). Similarly

$$\bar{u}'(\vec{p}',\sigma')\sigma_{ij}\gamma_5 u(\vec{p},\sigma) = -\epsilon_{ijk}\,\bar{u}'(\vec{p}',\sigma')\sigma_{k4}u(\vec{p},\sigma)\,, \tag{107}$$

with $\eta_{\sigma_{ij}\gamma_5} = +$.

B.2.2 Bilinears – unpolarised/polarised cases

Useful combinations discussed here are

- $\Gamma^{\rm unpol} = (1+\gamma_4)/2$ giving

$$\bar{u}'(\vec{p}',\sigma')\Gamma^{\rm unpol}u(\vec{p},\sigma) = s's\,\delta_{\sigma'\sigma}\,, \tag{108}$$

- $\Gamma^{\rm pol}_{\pm 3} = (1+\gamma_4)/2 \times (1 \pm i\gamma_5\gamma_3)$ giving

$$\bar{u}'(\vec{p}',\sigma')\Gamma^{\rm pol}_{\pm 3}u(\vec{p},\sigma) = s's\,(1\pm\sigma)\,\delta_{\sigma'\sigma}\,, \tag{109}$$

- $\Gamma^{\rm pol}_{\pm} = (1+\gamma_4)/2 \times i\gamma_5(\gamma_1 \pm i\gamma_2)$ giving

$$\bar{u}'(\vec{p}',\sigma')\Gamma^{\rm pol}_{\pm}u(\vec{p},\sigma) = s's\,(1\mp\sigma)\,\delta_{\sigma',-\sigma}\,. \tag{110}$$

C Alternative derivation of energy states for the $d_S = 2$ case

We give here an alternative derivation of the energy states in section 4 and in particular eqs. (53), (54) which does not depend on the choice of a particular Γ matrix choice in section 3.4. In eq. (39) we now have a $(2\times2)\times(2\times2)$ (i.e. $d_S = 2$) matrix to diagonalise.

Including the spin index we now have

$$\langle B_r(\vec{p}_r,\sigma_r)|\hat{\tilde{\mathcal{O}}}(\vec{q})|B_s(\vec{p}_s,\sigma_s)\rangle = \begin{pmatrix} 0 & a^\dagger \\ a & 0 \end{pmatrix}_{\sigma_r r,\sigma_s s}\,, \tag{111}$$

where a is replaced by a 2×2 matrix (and the complex conjugate a^* by the Hermitian conjugate $a^\dagger$). Thus, using eq. (88) we replace

$$a \to \begin{pmatrix} a_{++} & a_{+-} \\ a_{+-} & a_{--} \end{pmatrix}, \tag{112}$$

with $a_{-+} = -\eta a^*_{+-}$ and $a_{--} = \eta a_{++}$ where η is given in Table 3. The eigenvalues of the resulting enlarged D matrix in eq. (39) are easily found, by first writing D as a product of 2×2 sub-matrices as in eq. (131) and then taking the determinant with the identification $A \to \epsilon_1 I$, $B \to \epsilon_2 I$, $C \to a^\dagger$ and $D \to a$. We now have to solve the eigenvalue equation

$$\det\left((\epsilon_1-\mu)(\epsilon_2-\mu)I - \lambda^2 aa^\dagger\right) = 0\,, \tag{113}$$

for μ. Furthermore note that

$$aa^\dagger = (|a_{++}|^2 + |a_{+-}|^2)I = |\det a| I\,, \tag{114}$$

which is diagonal. So this means that each eigenvalue is doubly degenerate as expected (the double energy degeneracy) and leads to the replacement in eqs. (52), (54) of

$$|a| \to |\det a|^{1/2}\,, \tag{115}$$

(or $|a| \to (|a_{++}|^2 + |a_{+-}|^2)^{1/2}$), together with the appropriate change in $\kappa_\pm$.

Matrix elements are either unpolarised or polarised (including spin flip) and either real or imaginary. But one of these corresponds to a matrix element picked out by a Γ matrix in section 3.4. For example for $\Gamma^{\rm unpol}$ from eq. (45) where we have the replacement $a \to (a_{++}+a_{--})/2$ which also gives one matrix element for $|a|^2$ (i.e. $|a_{++}|^2$). Thus eq. (115) may be considered the general result. Additionally the eigenvectors are found to be

$$e^{(\pm\sigma)}_{\sigma_r r} = \frac{1}{\sqrt{\Delta E_\lambda}} \begin{pmatrix} \sqrt{\kappa_\pm}\delta_{\sigma_r\sigma} \\ \pm\,\mathrm{sgn}(\lambda)\sqrt{\kappa_\mp}\,\frac{a_{\sigma_r\sigma}}{\sqrt{|\det a|}} \end{pmatrix}_r . \tag{116}$$

Parallel to eq. (46) we have

$$C_{\lambda\, r\alpha, s\beta}(t) = \sum_{i=\pm}\sum_{\sigma=\pm} w^{(i\sigma)}_{r\alpha}\bar{w}^{(i\sigma)}_{s\beta} e^{-E^{(i)}_\lambda t}\,, \tag{117}$$

with

$$\begin{aligned} w^{(i\sigma)}_{r\alpha} &= \sum_{\sigma_r} {}_\lambda\langle 0|\hat{B}_{r\alpha}(\vec{0})|B_r(\vec{p}_r,\sigma_r)\rangle_\lambda\, e^{(i\sigma)}_{\sigma_r r}\,, \\ \bar{w}^{(i\sigma)}_{s\beta} &= \sum_{\sigma_s} {}_\lambda\langle B_s(\vec{p}_s,\sigma_s)|\hat{\bar{B}}_{s\beta}(\vec{0})|0\rangle_\lambda e^{(i\sigma)\,*}_{\sigma_s s}\,. \end{aligned} \tag{118}$$

Using eq. (41) gives

$$C^\Gamma_{\lambda\, rs}(t) = Z_r\bar{Z}_s \sum_{i=\pm}\sum_{\sigma=\pm}\sum_{\sigma_r\sigma_s} \bar{u}^{(s)}(\vec{p}_s,\sigma_s)\Gamma u^{(r)}(\vec{p}_r,\sigma_r) e^{(i\sigma)}_{\sigma_r r} e^{(i\sigma)\,*}_{\sigma_s s} e^{-E^{(i)}_\lambda t}\,. \tag{119}$$

However using eq. (116) we have

$$\sum_{\sigma=\pm} e^{(\pm\sigma)}_{\sigma_r r} e^{(\pm\sigma)\,*}_{\sigma_s s} = \frac{1}{\Delta E_\lambda} \begin{pmatrix} \kappa_\pm \delta_{\sigma_r\sigma_s} & \pm\lambda a^\dagger_{\sigma_r\sigma_s} \\ \pm\lambda a_{\sigma_r\sigma_s} & \kappa_\mp \delta_{\sigma_r\sigma_s} \end{pmatrix}_{rs} . \tag{120}$$

With no spin index we use the result of eq. (55) to give

$$e^{(\pm)}_r \, e^{(\pm)\,*}_s = \frac{1}{\Delta E_\lambda} \begin{pmatrix} \kappa_\pm & \pm\lambda a^*_\pm \\ \pm\lambda a_\pm & \kappa_\mp \end{pmatrix}_{rs} . \tag{121}$$

which with the substitutions of eqs. (112), (115) gives the spin case result in eq. (120).

More concretely if we set $\Gamma = \Gamma^{\rm unpol}$ and use eq. (44) and eq. (120) in eq. (119) and then re-write it using eq. (121) this soon leads to eq. (46) with $a \to (a_{++} + a_{--})/2$ as found there. A similar result holds for $\Gamma = \Gamma^{\rm pol}_3$. However this equivalence between the results with spin and without spin is because as mentioned previously both eqs. (108) and (109) are diagonal in σ_r, σ_s. If we consider a case where this is not true, for example $\Gamma^{\rm pol}_\pm$, eq. (110) then we soon find that[13]

$$C^{\Gamma^{\rm pol}_+}_{rs}(t) = Z_r \bar{Z}_s \frac{\lambda}{\Delta E_\lambda} \begin{pmatrix} 0 & a^*_{+-} \\ a_{+-} & 0 \end{pmatrix}_{rs} \left(e^{-E^{(+)}_\lambda t} - e^{-E^{(-)}_\lambda t} \right) , \tag{122}$$

(and similarly for $\Gamma^{\rm pol}_-$ with a_{+-} replaced by a_{-+}). The diagonal terms have now vanished, so it cannot be re-written as for the spinless case. Not only that but we now have a difference of two exponentials (rather than a sum). Expanding gives

$$C^{\Gamma^{\rm pol}_+}_{rs}(t) = Z_r \bar{Z}_s \lambda \begin{pmatrix} 0 & a^*_{+-} \\ a_{+-} & 0 \end{pmatrix}_{rs} t e^{-\bar{E}t} , \tag{123}$$

close to the form of the original Dyson expansion as discussed in section 3.4.

D Correlation functions

The correlation functions in eq. (61) are defined by

$$\begin{aligned} C_{\lambda\Sigma\Sigma}(t) &= {\rm tr}_D \Gamma \langle \tilde{B}_\Sigma(t;\vec{p}) \bar{B}_\Sigma(0,\vec{0}) \rangle_\lambda , \\ C_{\lambda\Sigma N}(t) &= {\rm tr}_D \Gamma \langle \tilde{B}_\Sigma(t;\vec{p}) \bar{B}_N(0,\vec{0}) \rangle_\lambda , \\ C_{\lambda N\Sigma}(t) &= {\rm tr}_D \Gamma \langle \tilde{B}_N(t;\vec{p}+\vec{q}) \bar{B}_\Sigma(0,\vec{0}) \rangle_\lambda , \\ C_{\lambda NN}(t) &= {\rm tr}_D \Gamma \langle \tilde{B}_N(t;\vec{p}+\vec{q}) \bar{B}_N(0,\vec{0}) \rangle_\lambda , \end{aligned} \tag{124}$$

[13] Again we have redefined Z_r and $\bar{Z}_s$ as in footnote 6.

with baryon wavefunctions given by

$$\tilde{B}_{\Sigma_\alpha}(t;\vec{p}) = \int_{\vec{x}} e^{-i\vec{p}\cdot\vec{x}} B_{\Sigma_\alpha}(t,\vec{x}) = \sum_{\vec{x}} e^{-i\vec{p}\cdot\vec{x}} \epsilon^{abc} d^a_\alpha(x) \left[d^b(x)^{T_D} C\gamma_5 s^c(x) \right] ,$$
$$\tilde{B}_{N_\alpha}(t;\vec{p}) = \int_{\vec{x}} e^{-i\vec{p}\cdot\vec{x}} B_{N_\alpha}(t,\vec{x}) = \sum_{\vec{x}} e^{-i\vec{p}\cdot\vec{x}} \epsilon^{abc} d^a_\alpha(x) \left[d^b(x)^{T_D} C\gamma_5 u^c(x) \right] , \quad (125)$$

(α is a Dirac index, a is a colour index and $C = \gamma_4\gamma_2$). As in eq. (61) we have taken a trace over the Dirac indices with $\Gamma = \Gamma^{\mathrm{unpol}}$. For the diagonal correlation functions this gives

$$C_{\lambda\,\Sigma\Sigma}(t) = \sum_{\vec{x}} e^{-i\vec{p}\cdot\vec{x}} \epsilon_{abc}\epsilon_{a'b'c'} \left\langle \mathrm{tr}_D \left[\Gamma G^{(dd)aa'}(\vec{x},t;\vec{0},0) \right] \mathrm{tr}_D \left[\tilde{G}^{(ss)bb'}(\vec{x},t;\vec{0},0) G^{(dd)cc'}(\vec{x},t;\vec{0},0) \right] + \mathrm{tr}_D \left[\Gamma G^{(dd)aa'}(\vec{x},t;\vec{0},0) \tilde{G}^{(ss)bb'}(\vec{x},t;\vec{0},0) G^{(dd)cc'}(\vec{x},t;\vec{0},0) \right] \right\rangle , \quad (126)$$

and

$$C_{\lambda\,NN}(t) = \sum_{\vec{x}} e^{-i(\vec{p}+\vec{q})\cdot\vec{x}} \epsilon_{abc}\epsilon_{a'b'c'} \left\langle \mathrm{tr}_D \left[\Gamma G^{(dd)aa'}(\vec{x},t;\vec{0},0) \right] \mathrm{tr}_D \left[\tilde{G}^{(uu)bb'}(\vec{x},t;\vec{0},0) G^{(dd)cc'}(\vec{x},t;\vec{0},0) \right] + \mathrm{tr}_D \left[\Gamma G^{(dd)aa'}(\vec{x},t;\vec{0},0) \tilde{G}^{(uu)bb'}(\vec{x},t;\vec{0},0) G^{(dd)cc'}(\vec{x},t;\vec{0},0) \right] \right\rangle , \quad (127)$$

where we have defined a tilde by $\tilde{X} = (C\gamma_5 X \gamma_5)^{T_D}$. For the off-diagonal correlation functions we have

$$C_{\lambda\,\Sigma N}(t) = \sum_{\vec{x}} e^{-i\vec{p}\cdot\vec{x}} \epsilon^{abc}\epsilon^{a'b'c'} \left\langle \mathrm{tr}_D \left[\Gamma G^{(dd)aa'}(\vec{x},t;\vec{0},0) \right] \mathrm{tr}_D \left[\tilde{G}^{(su)bb'}(\vec{x},t;\vec{0},0) G^{(dd)cc'}(\vec{x},t;\vec{0},0) \right] + \mathrm{tr}_D \left[\Gamma G^{(dd)aa'}(\vec{x},t;\vec{0},0) \tilde{G}^{(su)bb'}(\vec{x},t;\vec{0},0) G^{(dd)cc'}(\vec{x},t;\vec{0},0) \right] \right\rangle , \quad (128)$$

and similarly

$$C_{\lambda\,N\Sigma}(t) = \sum_{\vec{x}} e^{-i(\vec{p}+\vec{q})\cdot\vec{x}} \epsilon^{abc}\epsilon^{a'b'c'} \left\langle \mathrm{tr}_D \left[\Gamma G^{(dd)aa'}(\vec{x},t;\vec{0},0) \right] \mathrm{tr}_D \left[\tilde{G}^{(us)bb'}(\vec{x},t;\vec{0},0) G^{(dd)cc'}(\vec{x},t;\vec{0},0) \right] + \mathrm{tr}_D \left[\Gamma G^{(dd)aa'}(\vec{x},t;\vec{0},0) \tilde{G}^{(us)bb'}(\vec{x},t;\vec{0},0) G^{(dd)cc'}(\vec{x},t;\vec{0},0) \right] \right\rangle . \quad (129)$$

For simplicity we have taken the source for the Green's functions at $(\vec{0},0)$. For the more general smeared sources considered here we have

$$\sum_{\vec{x}} e^{-i\vec{p}\cdot\vec{x}} \ldots G(\vec{x},t;\vec{0},0) \ldots \to \sum_{\vec{x}_0} f(\vec{x}_0) \sum_{\vec{x}} e^{-i\vec{p}\cdot(\vec{x}-\vec{x}_0)} \ldots G(\vec{x},t;\vec{x}_0,0) \ldots . \quad (130)$$

E The fermion matrix inversion

We give here some more details of the procedure described in section 5.1.

E.1 General

To invert $\mathcal{M}$ in general we have

$$\begin{pmatrix} A & C \\ D & B \end{pmatrix} = \begin{pmatrix} A & 0 \\ D & I \end{pmatrix} \begin{pmatrix} I & A^{-1}C \\ D & B - DA^{-1}C \end{pmatrix}, \tag{131}$$

which gives

$$\begin{pmatrix} A & C \\ D & B \end{pmatrix}^{-1} = \begin{pmatrix} (A - CB^{-1}D)^{-1} & -A^{-1}C(B - DA^{-1}C)^{-1} \\ -B^{-1}D(A - CB^{-1}D)^{-1} & (B - DA^{-1}C)^{-1} \end{pmatrix}. \tag{132}$$

Equivalent forms, as can be seen by expanding the off-diagonal elements as a power series, is to re-write them as

$$\begin{aligned} B^{-1}D(A - CB^{-1}D)^{-1} &= (B - DA^{-1}C)^{-1}DA^{-1}, \\ A^{-1}C(B - DA^{-1}C)^{-1} &= (A - CB^{-1}D)^{-1}CB^{-1}. \end{aligned} \tag{133}$$

(Other variations are possible.) Note that we never need that C^{-1}, D^{-1} exist.

E.2 Specific

Thus here we have

$$A \to D_u, \quad B \to D_s, \quad C \to -\lambda\mathcal{T}, \quad D \to -\lambda\gamma_5\mathcal{T}^\dagger\gamma_5, \tag{134}$$

giving

$$\begin{aligned} &\mathcal{M}^{-1} \\ &= \begin{pmatrix} (\mathcal{M}^{-1})_{uu} & (\mathcal{M}^{-1})_{us} \\ (\mathcal{M}^{-1})_{su} & (\mathcal{M}^{-1})_{ss} \end{pmatrix} \\ &= \begin{pmatrix} (D_u - \lambda^2\mathcal{T}D_s^{-1}\gamma_5\mathcal{T}^\dagger\gamma_5)^{-1} & \lambda D_u^{-1}\mathcal{T}(D_s - \lambda^2\gamma_5\mathcal{T}^\dagger\gamma_5 D_u^{-1}\mathcal{T})^{-1} \\ \lambda D_s^{-1}\gamma_5\mathcal{T}^\dagger\gamma_5(D_u - \lambda^2\mathcal{T}D_s^{-1}\gamma_5\mathcal{T}^\dagger\gamma_5)^{-1} & (D_s - \lambda^2\gamma_5\mathcal{T}^\dagger\gamma_5 D_u^{-1}\mathcal{T})^{-1} \end{pmatrix}. \end{aligned} \tag{135}$$

Hence we have, upon re-writing

$$\begin{aligned} G^{(uu)} &= (1 - \lambda^2 D_u^{-1}\mathcal{T}D_s^{-1}\gamma_5\mathcal{T}^\dagger\gamma_5)^{-1}D_u^{-1}, \\ G^{(ss)} &= (1 - \lambda^2 D_s^{-1}\gamma_5\mathcal{T}^\dagger\gamma_5 D_u^{-1}\mathcal{T})^{-1}D_s^{-1}, \end{aligned} \tag{136}$$

and

$$\begin{aligned} G^{(us)} &= \lambda D_u^{-1}\mathcal{T}G^{(ss)}, \\ G^{(su)} &= \lambda D_s^{-1}\gamma_5\mathcal{T}^\dagger\gamma_5 G^{(uu)}, \end{aligned} \tag{137}$$

as given in the main text. Note that, as built in, we have

$$\gamma_5 G^{(su)\,\dagger}\gamma_5 = G^{(us)}. \tag{138}$$

References

[1] Y. Aoki et al., *FLAG Review 2021*, Eur. Phys. J. C **82** (2022) 869, [arXiv:2111.09849 [hep-lat]].

[2] A. S. Meyer, A. Walker-Loud and C. Wilkinson, *Status of Lattice QCD Determination of Nucleon Form Factors and their Relevance for the Few-GeV Neutrino Program*, Ann. Rev. Nucl. Part. Sci. 72 (2022) 205, [arXiv:2201.01839 [hep-lat]].

[3] D. Djukanovic, *Recent progress on nucleon form factors*, PoS **LATTICE2021** (2022) 009, arXiv:2112.00128 [hep-lat].

[4] K. U. Can, *Lattice QCD study of the elastic and transition form factors of charmed baryons*, Int. J. Mod. Phys. A **36** (2021) 2130013, [arXiv:2107.13159 [hep-lat]].

[5] M. Constantinou et al., *Parton distributions and lattice-QCD calculations: Toward 3D structure*, Prog. Part. Nucl. Phys. **121** (2021) 103908, [arXiv:2006.08636 [hep-ph]].

[6] K. Cichy and M. Constantinou, *A guide to light-cone PDFs from Lattice QCD: an overview of approaches, techniques and results*, Adv. High Energy Phys. **2019** (2019) 3036904, [arXiv:1811.07248 [hep-lat]].

[7] P. Gambino, S. Hashimoto, S. Mächler, M. Panero, F. Sanfilippo, S. Simula, A. Smecca and N. Tantalo, *Lattice QCD study of inclusive semileptonic decays of heavy mesons*, [arXiv:2203.11762 [hep-lat]].

[8] A. J. Chambers, R. Horsley, Y. Nakamura, H. Perlt, P. E. L. Rakow, G. Schierholz, A. Schiller, K. Somfleth, R. D. Young and J. M. Zanotti, *Nucleon Structure Functions from Operator Product Expansion on the Lattice*, [QCDSF Collaboration], Phys. Rev. Lett. **118** (2017) 242001, [arXiv:1703.01153 [hep-lat]].

[9] K. F. Liu, *Parton Distribution Function from the Hadronic Tensor on the Lattice*, PoS **LATTICE2015** (2016) 115, arXiv:1603.07352 [hep-ph].

[10] C. Y. Seng, D. Galviz, W. J. Marciano and U. G. Meißner, *Update on $|V_{us}|$ and $|V_{us}/V_{ud}|$ from semileptonic kaon and pion decays*, Phys. Rev. D **105** (2022) 013005, [arXiv:2107.14708 [hep-ph]].

[11] S. Gottlieb, *Lattice QCD Impact on Determination of CKM Matrix: Status and Prospects*, PoS **LATTICE2019** (2020) 275, arXiv:2002.09013 [hep-lat].

[12] Z. Davoudi, W. Detmold, K. Orginos, A. Parreño, M. J. Savage, P. Shanahan and M. L. Wagman, *Nuclear matrix elements from lattice QCD for electroweak and beyond-Standard-Model processes*, Phys. Rept. **900** (2021) 1, [arXiv:2008.11160 [hep-lat]].

[13] N. Severijns, M. Beck and O. Naviliat-Cuncic, *Tests of the standard electroweak model in beta decay*, Rev. Mod. Phys. **78** (2006) 991, [arXiv:nucl-ex/0605029 [nucl-ex]].

[14] M. González-Alonso, O. Naviliat-Cuncic and N. Severijns, *New physics searches in nuclear and neutron β decay*, Prog. Part. Nucl. Phys. **104** (2019) 165, [arXiv:1803.08732 [hep-ph]].

[15] V. Cirigliano, W. Detmold, A. Nicholson and P. Shanahan, *Lattice QCD Inputs for Nuclear Double Beta Decay*, Prog. Part. Nucl. Phys. **112** (2020) 103771 [arXiv:2003.08493 [nucl-th]].

[16] R. E. Smail, M. Batelaan, R. Horsley, Y. Nakamura, H. Perlt, D. Pleiter, P. E. L. Rakow, G. Schierholz, H. Stüben, R. D. Young and J. M. Zanotti, [QCDSF/UKQCD/CSSM Collaboration], *Constraining beyond the Standard Model nucleon isovector charges*, [arXiv:2304.02866 [hep-lat]].

[17] R. Horsley, R. Millo, Y. Nakamura, H. Perlt, D. Pleiter, P. E. L. Rakow, G. Schierholz, A. Schiller, F. Winter and J. M. Zanotti, [QCDSF-UKQCD Collaboration], *A Lattice Study of the Glue in the Nucleon*, Phys. Lett. B **714** (2012) 312, [arXiv:1205.6410 [hep-lat]].

[18] A. J. Chambers, R. Horsley, Y. Nakamura, H. Perlt, D. Pleiter, P. E. L. Rakow, G. Schierholz, A. Schiller, H. Stüben, R. D. Young and J. M. Zanotti, [CSSM and QCDSF/UKQCD Collaborations], *Feynman–Hellmann approach to the spin structure of hadrons*, Phys. Rev. D **90** (2014) 014510, [arXiv:1405.3019 [hep-lat]].

[19] A. J. Chambers, R. Horsley, Y. Nakamura, H. Perlt, D. Pleiter, P. E. L. Rakow, G. Schierholz, A. Schiller, H. Stüben, R. D. Young and J. M. Zanotti, *Disconnected contributions to the spin of the nucleon*, Phys. Rev. D **92** (2015) 114517, [arXiv:1508.06856 [hep-lat]].

[20] C. Bouchard, C. C. Chang, T. Kurth, K. Orginos and A. Walker-Loud, *On the Feynman–Hellmann Theorem in Quantum Field Theory and the Calculation of Matrix Elements*, Phys. Rev. D **96** (2017) 014504, [arXiv:1612.06963 [hep-lat]].

[21] A. J. Chambers, J. Dragos, R. Horsley, Y. Nakamura, H. Perlt, D. Pleiter, P. E. L. Rakow, G. Schierholz, A. Schiller, K. Somfleth, H. Stüben,

R. D. Young and J. Zanotti [QCDSF, UKQCD and CSSM], *Electromagnetic form factors at large momenta from lattice QCD*, Phys. Rev. D **96** (2017) 114509, [arXiv:1702.01513 [hep-lat]].

[22] M. Lüscher and U. Wolff, *How to Calculate the Elastic Scattering Matrix in Two-dimensional Quantum Field Theories by Numerical Simulation*, Nucl. Phys. B **339** (1990) 222.

[23] B. Blossier, M. Della Morte, G. von Hippel, T. Mendes and R. Sommer, *On the generalized eigenvalue method for energies and matrix elements in lattice field theory*, JHEP **04** (2009) 094, [arXiv:0902.1265 [hep-lat]].

[24] B. J. Owen, J. Dragos, W. Kamleh, D. B. Leinweber, M. S. Mahbub, B. J. Menadue and J. M. Zanotti, *Variational Approach to the Calculation of g_A*, Phys. Lett. B **723** (2013) 217, [arXiv:1212.4668 [hep-lat]].

[25] D. Guadagnoli, V. Lubicz, M. Papinutto and S. Simula, *First Lattice QCD Study of the $\Sigma^- \to n$ Axial and Vector Form Factors with $SU(3)$ Breaking Corrections*, Nucl. Phys. B **761** (2007) 63, [arXiv:hep-ph/0606181].

[26] P. E. Shanahan, A. N. Cooke, R. Horsley, Y. Nakamura, P. E. L. Rakow, G. Schierholz, A. W. Thomas, R. D. Young and J. M. Zanotti, *SU(3) breaking in hyperon transition vector form factors*, Phys. Rev. D **92** (2015) 074029, [arXiv:1508.06923 [nucl-th]].

[27] S. Sasaki, *Continuum limit of hyperon vector coupling $f_1(0)$ from $2+1$ flavor domain wall QCD*, Phys. Rev. D **96** (2017) 074509, [arXiv:1708.04008 [hep-lat]].

[28] J. M. Bickerton, A. N. Cooke, R. Horsley, Y. Nakamura, H. Perlt, D. Pleiter, P. E. L. Rakow, G. Schierholz, H. Stüben, R. D. Young, and J. M. Zanotti, [QCDSF-UKQCD-CSSM Collaboration], *Patterns of flavour symmetry breaking in hadron matrix elements involving u, d and s quarks*, PoS **LATTICE2021** (2022) 490, arXiv:2112.04445 [hep-lat].

[29] R. Horsley, M. Batelaan, K. U. Can, Y. Nakamura, H. Perlt, P. E. L. Rakow, G. Schierholz, H. Stüben, R. D. Young and J. M. Zanotti [QCDSF-UKQCD-CSSM Collaborations], *Quasi-degenerate baryon energy states, the Feynman-Hellmann theorem and transition matrix elements*, PoS **LATTICE2022** (2022) 412, arXiv:2302.04911 [hep-lat].

[30] M. Lüscher and P. Weisz, *Definition and General Properties of the Transfer Matrix in Continuum Limit Improved Lattice Gauge Theories*, Nucl. Phys. B **240** (1984) 349.

[31] K. U. Can, A. Hannaford-Gunn, R. Horsley, Y. Nakamura, H. Perlt, P. E. L. Rakow, G. Schierholz, K. Y. Somfleth, H. Stüben, R. D. Young and J. M. Zanotti [QCDSF/UKQCD/CSSM Collaborations], *Lattice evaluation of the Compton amplitude employing the Feynman–Hellmann theorem*, Phys. Rev. D **102** (2020) 114505, [arXiv:2007.01523 [hep-lat]].

[32] C. Best, M. Göckeler, R. Horsley, E. M. Ilgenfritz, H. Perlt, P. E. L. Rakow, A. Schäfer, G. Schierholz, A. Schiller and S. Schramm, *Pion and rho structure functions from lattice QCD*, Phys. Rev. D **56** (1997) 2743, [arXiv:hep-lat/9703014 [hep-lat]].

[33] K. U. Can [QCDSF/UKQCD Collaboration], *The Compton amplitude and nucleon structure functions*, PoS **LATTICE2022** (2023) 237, arXiv:2212.09197 [hep-lat].

[34] K. U. Can, A. Hannaford-Gunn, R. Horsley, Y. Nakamura, H. Perlt, P. E. L. Rakow, E. Sankey, G. Schierholz, H. Stüben, R. D. Young and J. M. Zanotti, *The Compton Amplitude, lattice QCD and the Feynman–Hellmann approach*, SciPost Phys. Proc. **6** (2022) 003, arXiv:2201.08367 [hep-lat].

[35] J. M. Bickerton, R. Horsley, Y. Nakamura, H. Perlt, D. Pleiter, P. E. L. Rakow, G. Schierholz, H. Stüben, R. D. Young and J. M. Zanotti [QCDSF-UKQCD-CSSM Collaboration], *Patterns of flavor symmetry breaking in hadron matrix elements involving u , d , and s quarks*, Phys. Rev. D **100** (2019) 114516, [arXiv:1909.02521 [hep-lat]].

[36] N. Cundy, M. Göckeler, R. Horsley, T. Kaltenbrunner, A. D. Kennedy, Y. Nakamura, H. Perlt, D. Pleiter, P. E. L. Rakow, A. Schäfer, G. Schierholz, A. Schiller, H. Stüben and J. M. Zanotti, [QCDSF-UKQCD Collaboration], *Non-perturbative improvement of stout-smeared three flavour clover fermions*, Phys. Rev. D **79** (2009) 094507, [arXiv:0901.3302 [hep-lat]].

[37] W. Bietenholz, V. Bornyakov, M. Göckeler, R. Horsley, W. G. Lockhart, Y. Nakamura, H. Perlt, D. Pleiter, P. E. L. Rakow, G. Schierholz, A. Schiller, T. Streuer, H. Stüben, F. Winter and J. M. Zanotti, [QCDSF-UKQCD Collaboration], *Flavour blindness and patterns of flavour symmetry breaking in lattice simulations of up, down and strange quarks*, Phys. Rev. D **8**4 (2011) 054509, [arXiv:1102.5300 [hep-lat]].

[38] P. F. Bedaque, *Aharonov-Bohm effect and nucleon nucleon phase shifts on the lattice*, Phys. Lett. B **593** (2004) 82, [arXiv:nucl-th/0402051 [nucl-th]].

[39] C. T. Sachrajda and G. Villadoro, *Twisted boundary conditions in lattice simulations*, Phys. Lett. B **609** (2005) 73, [arXiv:hep-lat/0411033 [hep-lat]].

[40] P. F. Bedaque and J. W. Chen, *Twisted valence quarks and hadron interactions on the lattice*, Phys. Lett. B **616** (2005) 208, [arXiv:hep-lat/0412023 [hep-lat]].

[41] J. M. Flynn, A. Jüttner, C. T. Sachrajda, P. A. Boyle and J. M. Zanotti, *Hadronic form factors in Lattice QCD at small and vanishing momentum transfer*, JHEP **05** (2007) 016, [arXiv:hep-lat/0703005 [hep-lat]].

[42] P. A. Boyle, J. M. Flynn, A. Jüttner, C. Kelly, H. P. de Lima, C. M. Maynard, C. T. Sachrajda and J. M. Zanotti, *The Pion's electromagnetic form-factor at small momentum transfer in full lattice QCD*, JHEP **07** (2008) 112, [arXiv:0804.3971 [hep-lat]].

[43] B. Yoon, R. Gupta, T. Bhattacharya, M. Engelhardt, J. Green, B. Joó, H. W. Lin, J. Negele, K. Orginos and A. Pochinsky, D. Richards, S. Syritsyn and F. Winter, [NME Collaboration], *Controlling Excited-State Contamination in Nucleon Matrix Elements*, Phys. Rev. D **9**3 (2016) 114506, [arXiv:1602.07737 [hep-lat]].

[44] M. Göckeler, T. R. Hemmert, R. Horsley, D. Pleiter, P. E. L. Rakow, A. Schäfer and G. Schierholz, [QCDSF Collaboration], *Nucleon electromagnetic form-factors on the lattice and in chiral effective field theory*, Phys. Rev. D **71** (2005) 034508, [arXiv:hep-lat/0303019 [hep-lat]].

[45] A. S. Wightman, *Three formulas for the off-diagonal density matrix of a Dirac spinor with an application*, J. Math. Phys. 42, **674** (2001) 674.

[46] P. B. Pal, *Representation-independent manipulations with Dirac spinors*, [arXiv:physics/0703214 [physics.ed-ph]].

[47] C. Lorcé, *New explicit expressions for Dirac bilinears*, Phys. Rev. D **97** (2018) 016005, [arXiv:1705.08370 [hep-ph]].

[48] M. A. Olpak and A. Ozpineci, *On the calculation of covariant expressions for Dirac bilinears*, Eur. Phys. J. C **81** (2021) 798, [arXiv:1905.10470 [hep-th]].

[49] J. Dragos, R. Horsley, W. Kamleh, D. B. Leinweber, Y. Nakamura, P. E. L. Rakow, G. Schierholz, R. D. Young and J. M. Zanotti, *Nucleon matrix elements using the variational method in lattice QCD*, Phys. Rev. D **94** (2016) 074505, [[arXiv:1606.03195 [hep-lat]].

[50] T. R. Haar, Y. Nakamura and H. Stüben, *An update on the BQCD Hybrid Monte Carlo program*, EPJ Web Conf. **175** (2018) 14011, [arXiv:1711.03836 [hep-lat]].

[51] R. G. Edwards and B. Joó, *The Chroma software system for lattice QCD*, Nucl. Phys. B Proc. Suppl. **140** (2005) 832, arXiv:hep-lat/0409003.

[52] M. Creutz, *Gauge Fixing, the Transfer Matrix, and Confinement on a Lattice*, Phys. Rev. D **15** (1977) 1128.

[53] I. Montvay and G. Münster *Quantum Fields on a Lattice*, Cambridge University Press 1994.